Miner Deposita (2009) 44:99–128
DOI 10.1007/s00126-008-0188-0

ARTICLE

The Rožná uranium deposit (Bohemian Massif, Czech Republic): shear zone-hosted, late Variscan and post-Variscan hydrothermal mineralization

Bohdan Kříbek · Karel Žák · Petr Dobeš · Jaromír Leichmann · Marta Pudilová · Miloš René · Bohdan Scharm · Marta Scharmová · Antonín Hájek · Daniel Holeczy · Ulrich F. Hein · Bernd Lehmann

Received: 10 January 2006 / Accepted: 8 April 2008 / Published online: 13 June 2008
© Springer-Verlag 2008

Abstract Three major mineralization events are recorded at the Rožná uranium deposit (total mine production of 23,000 t U, average grade of 0.24% U): (1) pre-uranium quartz-sulfide and carbonate-sulfide mineralization, (2) uranium, and (3) post-uranium quartz-carbonate-sulfide mineralization. (1) K–Ar ages for white mica from wall rock alteration of the pre-uranium mineralization style range from 304.5±5.8 to 307.6±6.0 Ma coinciding with the post-orogenic exhumation of the Moldanubian orogenic root and retrograde-metamorphic equilibration of the high-grade metamorphic host rocks. The fluid inclusion record consists of low-salinity aqueous inclusions, together with H_2O-CO_2-CH_4, CO_2-CH_4, and pure CH_4 inclusions. The fluid inclusion, paragenetic, and isotope data suggest that the pre-uranium mineralization formed from a reduced low-salinity aqueous fluid at temperatures close to 300°C. (2) The uraniferous hydrothermal event is subdivided into the pre-ore, ore, and post-ore substages. K–Ar ages of pre-ore authigenic K-feldspar range from 296.3±7.5 to 281.0±5.4 Ma and coincide with the transcurrent reorganization of crustal blocks of the Bohemian Massif and with Late Stephanian to Early Permian rifting. Massive hematitization, albitization, and desilicification of the pre-ore altered rocks indicate an influx of oxidized basinal fluids to the crystalline rocks of the Moldanubian domain. The wide range of salinities of fluid inclusions is interpreted as a result of the large-scale mixing of basinal brines with meteoric water. The cationic composition of these fluids

Editorial handling: M. Cuney

B. Kříbek (✉) · K. Žák · P. Dobeš
Czech Geological Survey,
Klárov 3,
118 21 Prague 1, Czech Republic
e-mail: kribek@cgu.cz

J. Leichmann
Faculty of Sciences, Masaryk University,
Kotlářská 2,
611 37 Brno, Czech Republic

M. Pudilová
Faculty of Sciences, Charles University,
Albertov 6,
128 43 Prague 2, Czech Republic

M. René
Institute of Rock Structure and Mechanics,
Academy of Sciences of the Czech Republic,
V Holešovičkách 41,
182 09 Prague 8, Czech Republic

B. Scharm · M. Scharmová
Jižní 63/19,
460 14 Liberec, Czech Republic

A. Hájek · D. Holeczy
Diamo, S. E., Branch GEAM,
592 51 Dolní Rožínka, Czech Republic

U. F. Hein
Octavia AG,
Marie-Calm Str. 1,
34131 Kassel, Germany

B. Lehmann
Institute of Mineralogy and Mineral Resources,
Technical University of Clausthal,
Adolph Roemer Str. 2A,
38678 Clausthal-Zellerfeld, Germany

indicates extensive interaction with crystalline rocks. Chlorite thermometry yielded temperatures of 260°C to 310°C. During this substage, uranium was probably leached from the Moldanubian crystalline rocks. The hydrothermal alteration of the ore substage followed, or partly overlapped in time, the pre-ore substage alteration. K–Ar ages of illite from ore substage alteration range from 277.2±5.5 to 264.0±4.3 Ma and roughly correspond with the results of chemical U–Pb dating of authigenic monazite (268±50 Ma). The uranium ore deposition was accompanied by large-scale decomposition of biotite and pre-ore chlorite to Fe-rich illite and iron hydrooxides. Therefore, it is proposed that the deposition of uranium ore was mostly in response to the reduction of the ore-bearing fluid by interaction with ferrous iron-bearing silicates (biotite and pre-ore chlorite). The Th data on primary, mostly aqueous, inclusions trapped in carbonates of the ore substage range between 152°C and 174°C and total salinity ranges over a relatively wide interval of 3.1 to 23.1 wt% NaCl eq. Gradual reduction of the fluid system during the post-ore substage is manifested by the appearance of a new generation of authigenic chlorite and pyrite. Chlorite thermometry yielded temperatures of 150°C to 170°C. Solid bitumens that post-date uranium mineralization indicate radiolytic polymerization of gaseous and liquid hydrocarbons and their derivatives. The origin of the organic compounds can be related to the diagenetic and catagenetic transformation of organic matter in Upper Stephanian and Permian sediments. (3) K–Ar ages on illite from post-uranium quartz-carbonate-sulfide mineralization range from 233.7±4.7 to 227.5±4.6 Ma and are consistent with the early Tethys-Central Atlantic rifting and tectonic reactivation of the Variscan structures of the Bohemian Massif. A minor part of the late Variscan uranium mineralization was remobilized during this hydrothermal event.

Keywords Uranium · Bohemian Massif · Rožná · Czech Republic

Introduction

The Bohemian Massif is a part of the Variscan belt of Central Europe and hosts many uranium deposits of various sizes, both in the Czech Republic and bordering eastern Germany (Fig. 1). The total historical uranium production is approximately 350,000 t (OECD-IAEA 2003) and makes the Bohemian Massif the most important uranium ore district in Europe. This paper deals with the Rožná deposit (a part of the Rožná-Olší uranium ore district, total mine production of 23,000 t U) located 45 km NW of Brno. The Rožná deposit was discovered in 1954 by a ground gamma-ray spectrometric survey and started production in 1957. At present, the mining operations reached the depth of 950 to 1,100 m with an average grade of 0.243% U and a cut-off grade of 0.04% U. The annual mine production is about 284 t U.

Numerous unpublished studies on the geology, mineralogy, and geochemistry of Rožná were summarized by Arapov et al. (1984) and Vilhelm et al. (1984). The uranium mineralization was dated at 280–260 Ma (U–Pb, uraninite; Anderson et al. 1988). Fluid inclusions in host rocks and ores were studied by Vosteen and Weinoldt (1997), Dobeš et al. (2001), and Hein et al. (2002). The isotope composition of carbonates and sulfides was determined by Žák et al. (2001). Selenide mineralization that accompanies uranium mineralization at Rožná was studied by Johan and colleagues (1971, 1976, 1978), and the rare earth element, yttrium and zircon mobility associated with uranium mineralization is discussed in René (2008). During the last 15 years, a detailed structural, petrological, mineralogical, and geochemical investigation of the deposit together with stable isotope, fluid inclusion, cathodoluminescence, and organic-geochemical research were performed to characterize structural, geochemical, and time controls on ore deposition. The results of this project, including primary data, were summarized by Kříbek and Hájek (2005), and a short version is presented in this paper. The aim of this comprehensive study is to characterize the sources of the uranium-bearing fluids and the *p–T* conditions of the successive fluid events during the post-orogenic evolution of the Bohemian Massif. The data allow to propose a descriptive model of the shear zone-hosted uranium mineralization and to relate its origin to the late Variscan and post-Variscan geological history of the Bohemian Massif.

Geological outline of the eastern part of the Bohemian Massif

The Rožná-Olší uranium ore district lies in the northeastern part of the Moldanubian domain of the Bohemian Massif (Fig. 2). The high-grade Moldanubian domain (Moldanubian sensu stricto) was overthrust on the north-easterly located medium-grade Moldanubian domain, i.e., the Svratka Crystalline Unit, and on the easterly located Cadomian Brunovistulian foreland consisting of unmetamorphosed and virtually undeformed Neoproterozoic granitoids emplaced into Neoproterozoic schists and migmatites. The large-scale thrust tectonics was responsible for the origin of two crystalline Brunovistulian foreland-derived nappes forming the so-called Moravian Zone (Matté et al. 1990; Schulmann et al. 1991). The high-grade Cambrian to Mid-Devonian metasedimentary and metavolcanic rock sequence of the Moldanubian domain represents an exhumed root of the Variscan orogenic belt (Franke 2006). It has been sub-

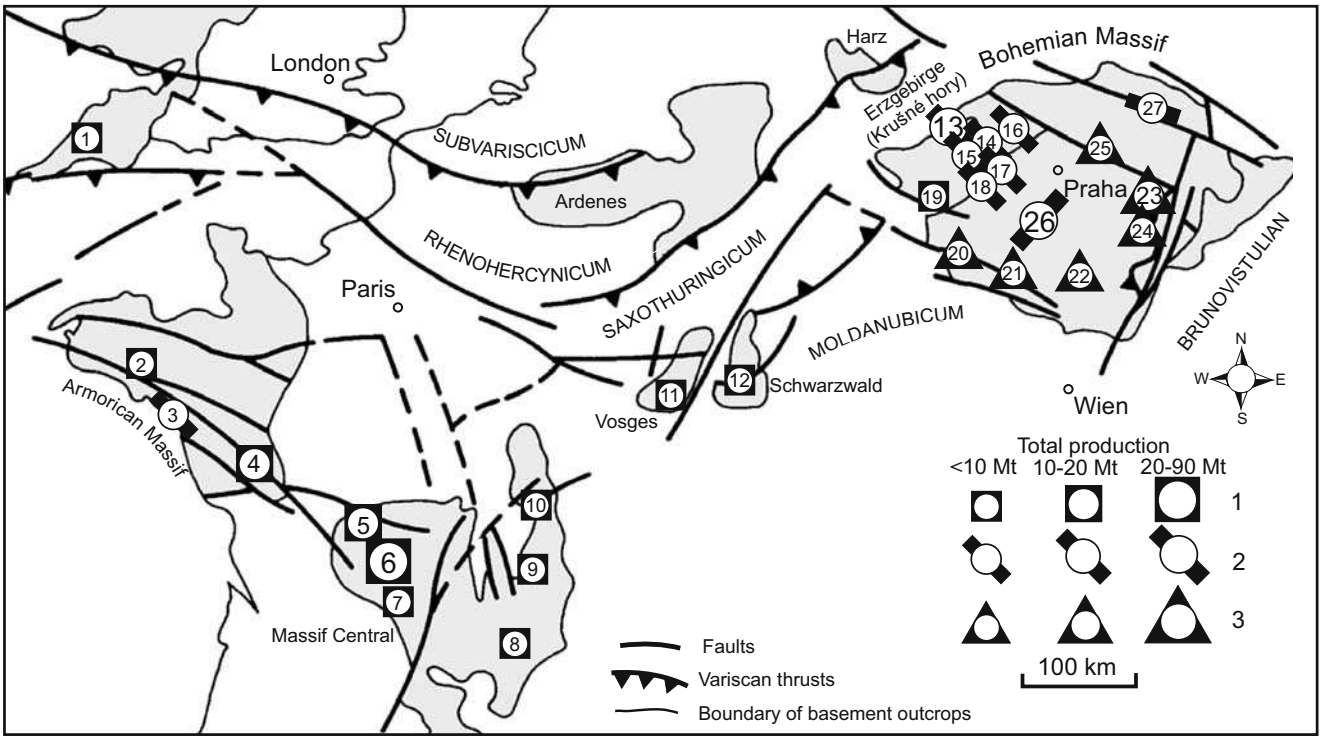


Fig. 1 Hydrothermal vein-type, fault-, and shear zone-hosted uranium deposits of the Variscan belts of western and central Europe. *1* Granite-hosted, vein- or fault-type deposit, important hydrothermal alteration (episyenite); *2* vein-type deposit, spatially associated with granite, weak alteration; *3* fault- or shear zone-type deposit, no evident association with granite, important alteration of crystalline host rocks. Uranium deposits and mining districts: *1* Cornwall 2,300 t U, South Terras deposit; *2* Bretagne, 1,100 t U, Bonote, Quistiave, Kerler, Rosglas, and Prat Merien deposits; *3* Penaran 470 t U; *4* Vendée, 14,470 t U, L'Escarpière, La Commanderie, Le Chardon, La Chapelle, and Largeau deposits; *5* Le Bernardan, 8,900 t U, Bernardan, Les Loges, and Mas Grimaud deposits; *6* La Crouzille, 23,600 t U, Le Brugeaud, Fanay, Margnac, Pèny, Le Fraisse, Bellezanne, and Henriete deposits; *7* Millevaches, 600 t U, Hyverneresse deposit; *8* Lozère, 3,540 t U, Le Cellier, Les Pierres Plantées, and Villeret deposits; *9* Forez, 7,170 t U, Bois Noirs-Limouzat, and Lachaux deposits; *10* Morvan, 1,390 t U, Jalerys, Les Brosses, and La Faye deposits; *11* Vosges, Kruth (never exploited); *12* Black Forest, Müllenbach deposit (never exploited); *13* Schlema-Alberoda, 88,000 t U; *14*. Johanngeorgenstadt deposit, 3,600 t U; *15* Pöhla-Tellerhäuser-Hämmerlein, 3,800 t U; *16* Annaberg deposit, 496 t U; *17* Jáchymov, 8,500 t U; *18* Horní Slavkov, 500 t U; *19* Grossschloppen deposit (never exploited); *20* Mähring deposit, 100 t U; *21* West Bohemian area, 9,800 t U, Zadní Chodov, Dyleň, and Vítkov II deposits; *22* Okrouhlá Radouň deposit, 1,300 t U; *23* Rožná-Olší, 23,000 t U, Rožná and Olší deposits; *24* Jasenice-Pucov, 450 t U; *25* Licoměřice deposit, 350 t U; *26* Příbram, 51,000 t U; *27* Lower Silesia, 500 t U, Kowary, Kletno, and Radoniów deposits

divided into the Monotonous Unit that consists of biotite-plagioclase paragneisses interlayered with leucocratic, K-feldspar-rich granitic orthogneisses, and the Varied Unit composed of a strongly deformed, thick sequence of biotite-plagioclase gneisses with garnet, sillimanite, and/or interlayered calc-silicate rocks, quartzite, intercalations of marble, graphite schists, and numerous bodies of amphibolites (Thiele 1976; Matura 1984; Fuchs 1986). Tollmann (1982) grouped the Monotonous and Varied Units into the so-called Drosendorf Unit, based on their relatively low degree of metamorphism compared to the overlying high-grade Gföhl Unit. The Gföhl Unit is formed by a large body of granitic gneiss associated with migmatites and K-feldspar-sillimanite paragneisses. It now represents the uppermost structural level of the Moldanubian domain and contains numerous bodies of kyanite-K-feldspar granulite (U–Pb zircon ages around 340 Ma; Kröner et al. 2000) and tectonic lenses of eclogite and garnet and/or spinel peridotite. Overthrusting of the Gföhl Unit over the less allochthonous Drosendorf Unit led to widespread metamorphism around 340 Ma (Franke 2006). Early post-metamorphic durbachites with U–Pb zircon ages between 338 and 335 Ma reflect HP melting in mantle or slab rocks (Kotková et al. 2003). During the early stage of post-orogenic extension in the Moldanubian domain (325 to 300 Ma; Handler et al. 1991) high-grade rocks were—to a variable degree—affected by a greenschist-facies overprint.

Geology of the Rožná uranium deposit

The Rožná deposit is located in the Gföhl Unit of the high-grade Moldanubian domain, close to its boundary with the medium-grade Svratka Crystalline Unit (Fig. 3). The tectonic boundary between the high-grade Gföhl Unit and the Svratka Crystalline Unit is interpreted as a low-angle

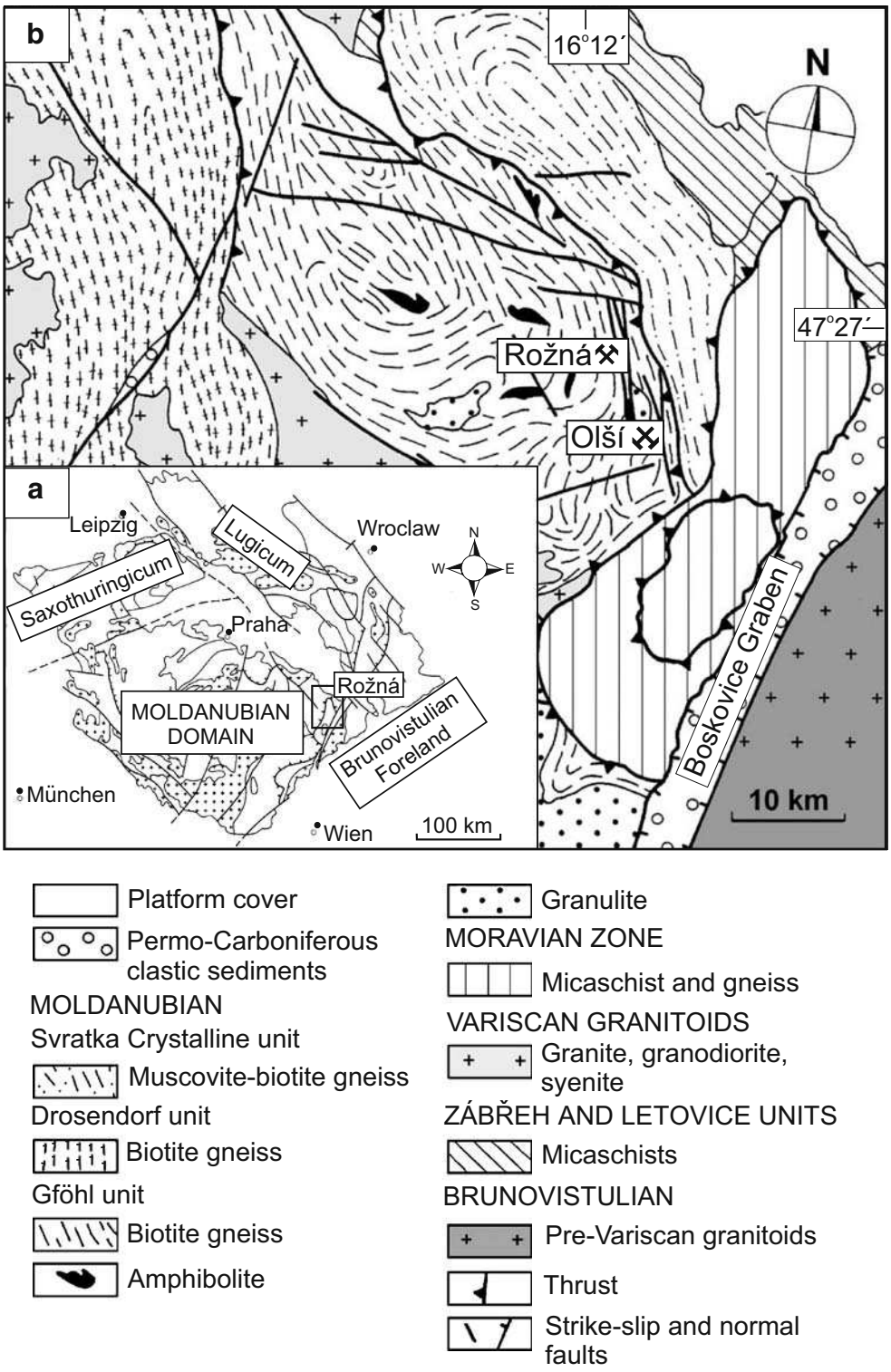


Fig. 2 (**a**) Location of the Rožná deposit in the Bohemian Massif. (**b**) Simplified geological map of the eastern margin of the Bohemian Massif with main tectonic units and major thrusts indicated

thrust between the two Moldanubian subunits (Tajčmanová et al. 2006). The host rocks of the Rožná deposit consist mainly of Bt+Plg+Kf+Qtz±Grt±Sill±Hbl gneisses and amphibolites with small bodies of calc-silicate gneiss, marble, serpentinite, and pyroxenite. Fine- to medium-grained biotite gneisses are the most abundant rock type and show ample evidence of anatexis (U–Pb zircon ages between 340 and 337 Ma; Schulmann et al. 2005). Partial melting of gneisses gave rise to distinctly banded, medium-grained, mostly stromatitic migmatites. Advanced partial melting of gneisses resulted in the formation of anatectic gneisses (anatectic granites). The Hbl+Plg±Grt±Bt±Cpx±

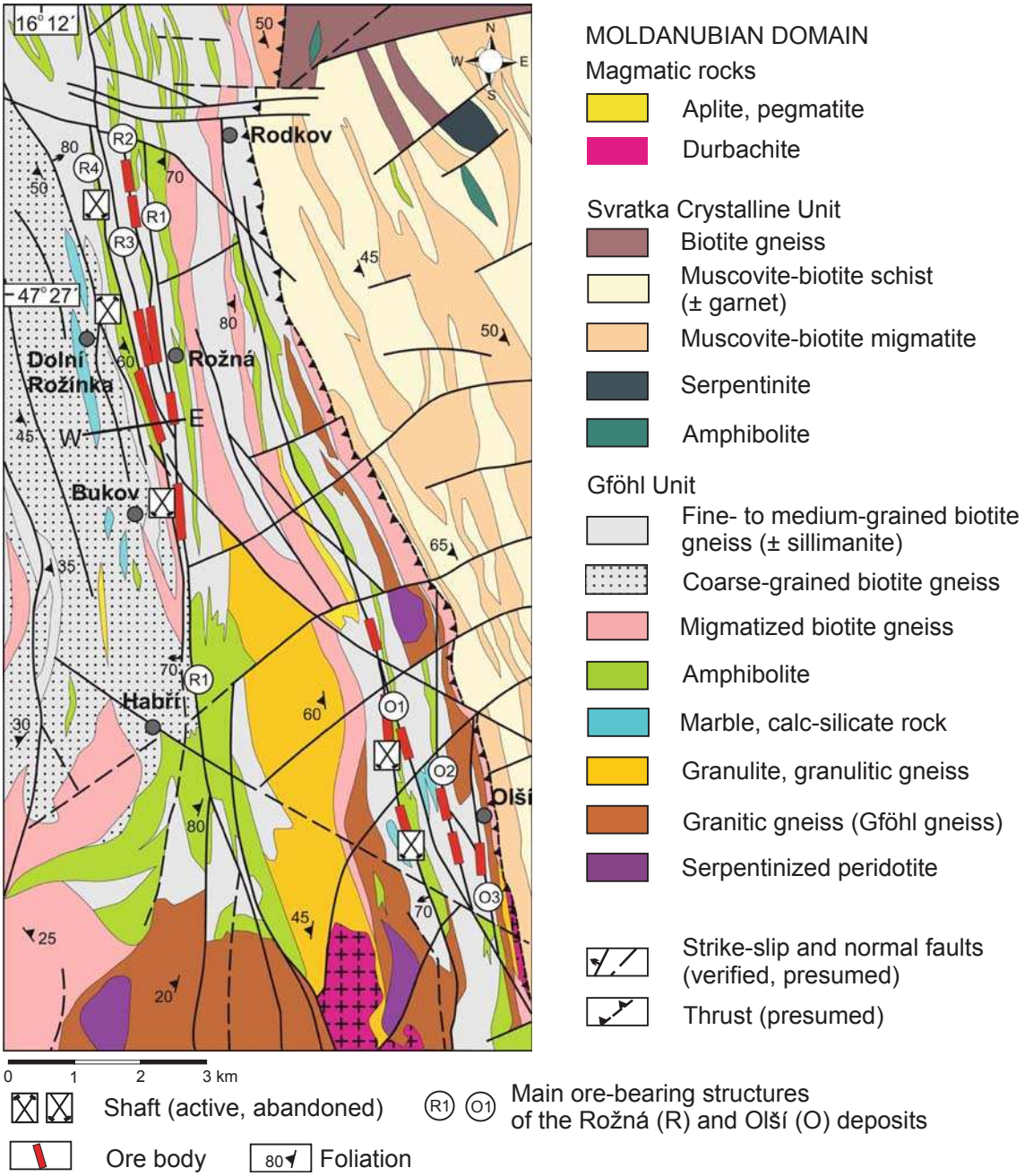


Fig. 3 Geological map of the Rožná-Olší ore district

Qtz±Tnt amphibolites, together with small lenses of pyroxenite, form bodies several centimeters to several meters thick, traceable over a distance of as much as several hundred meters. The Cpx+Qtz+Kfs+Plg±Grt±Hbl±Frs±Bt±Cal±Scp±Tnt calc-silicate gneisses form bodies up to 15 m thick and usually occur in association with marbles and amphibolites. Stratiform barite-hyalophane-sulfide and anhydrite-pyrite lenses form a part of the metasedimentary sequence (Kříbek et al. 1996, 2002).

Early, steep, NNW–SSE- to NNE–SSW-striking foliation in rocks of the Rožná deposit is interpreted as a result of E–W compression at lower crustal levels (Schulmann et al. 1999; Tajčmanová et al. 2006). The subsequent exhumation to middle crustal levels was associated with kilometer-scale isoclinal folding (Fig. 4). Fold axial planes strike N–S to NE–SW with an easterly or westerly vergence. Lineation of mineral elongation is developed parallel to NE–SW-trending fold axes. Longitudinal N–S- to NNW–SSE-striking ductile shear zones (Rožná and Olší shear zones) dip WSW at an angle of 70–90° and strike parallel to the tectonic contact between the Gföhl Unit and the Svratka Crystalline Unit (Fig. 3). The origin of the shear

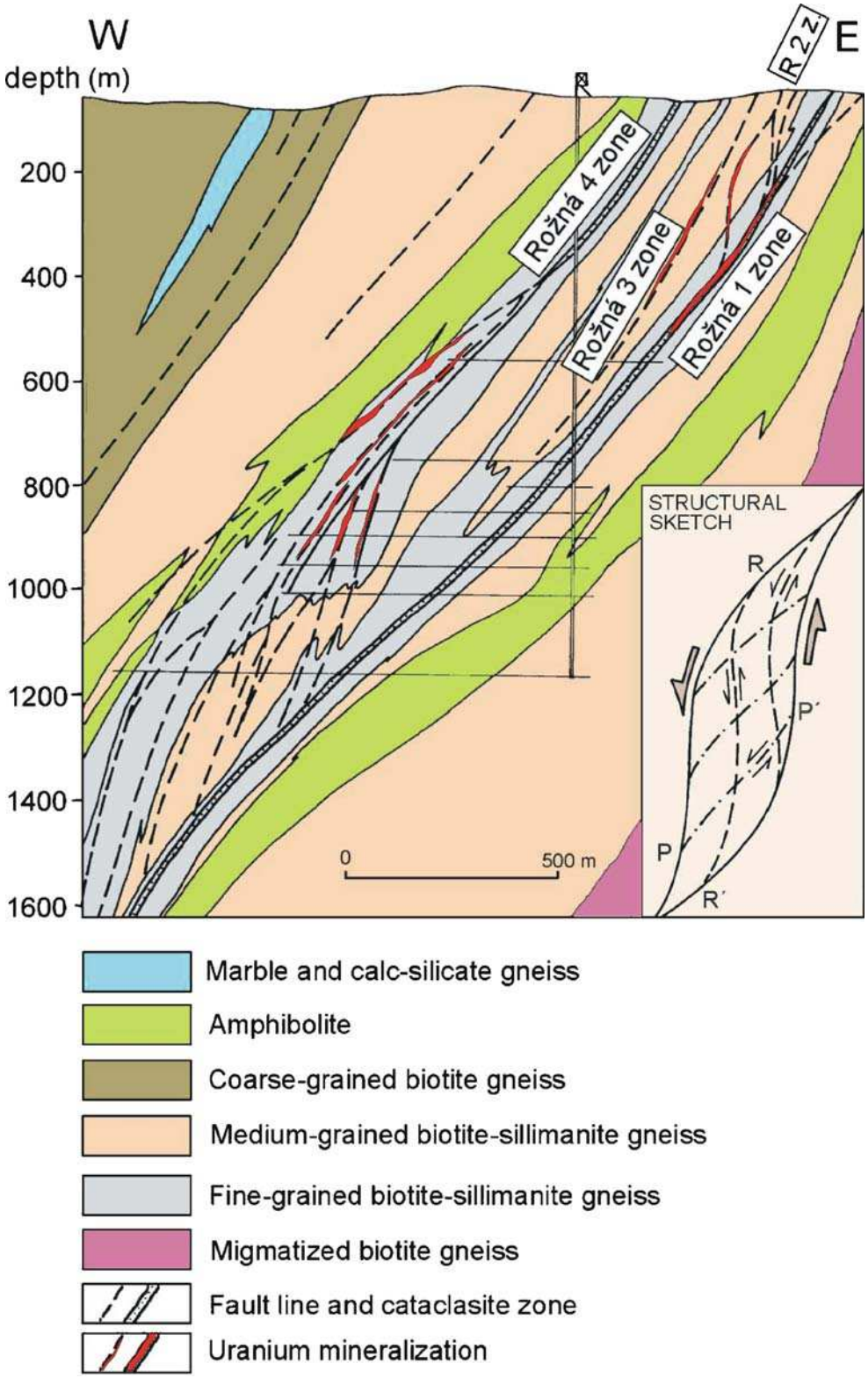


Fig. 4 Schematic geological cross-section of the Rožná uranium deposit and interpretation of the vertical movement component on major fault structures. Rožná 1 and Rožná 4: marginal faults of a shear zone, *R′–R*: planes of synthetic Riedel shears (pinnate structures), *P′–P*: compressional joints with no mineralization (not shown in the geological cross-section)

zones is compatible with SW–NE normal and N–S dextral kinematics (Kříbek and Hájek 2005). Superimposed, mostly normal zones of brittle deformation are associated with graphite- and phyllosilicate-rich coherent and incoherent cataclasites and fault breccias several centimeters to 15 m in thickness. The main longitudinal border faults of the Rožná shear zone are designated as Rožná 1 and Rožná 4 and host the main part of the disseminated uranium mineralization

(Figs. 3 and 4). The less strongly mineralized Rožná 2 and Rožná 3 fault zones and numerous separate pinnate carbonate veins can be interpreted as synthetic Riedel shear structures (Fig. 4).

Longitudinal fault structures hosting uranium mineralization are crosscut and segmented by steep, ductile to brittle NW–SE- and SW–NE-striking fault zones that host post-uranium carbonate-quartz-sulfide mineralization.

Ore bodies and macroscopic types of uranium mineralization

Uranium mineralization forms (1) disseminated coffinite>uraninite>U-Zr-silicate ore in chloritized, pyritized, carbonatized, and graphite-enriched cataclasites of longitudinal faults, (2) uraninite>coffinite ore in carbonate veins, (3) disseminated coffinite>uraninite ore in desilicified, albitized, and hematitized gneiss adjacent to longitudinal faults, and (4) mostly coffinite ore bound to the intersection of the longitudinal structures with oblique fault and joint systems.

(Ad 1) The main ore-bearing structures of Rožná are represented by fault zones R1 and R4 (Figs. 3 and 4). The zones comprise massive cataclasite 4–15 m thick or several subparallel cataclasite bodies 1–3 m thick, traceable over the horizontal distance of 15 km. The zones strike 340–355° and dip west at an angle of 45–70°. The ore is composed of uraninite, coffinite, (U,Zr)-silicates, and minor montroseite disseminated in chloritized, hematitized, limonitized, argillized, and pyritized coherent and incoherent cataclasites and fault breccias (Fig. 5a). Ore lenses are up to 90,000 m^2 large and are 3.5 m thick on average. The grade is around 0.5% U, up to 10% U locally.

(Ad 2) Ore zones R2 and R3 and carbonate veins represent pinnate structures genetically related to the master faults of the Rožná shear zone. These structures are traceable over a distance of 4–5 km and dip west at an angle of 55–90°. Compared to the master faults R1 and R4, they host a large number of carbonate veins up to 2 m thick with predominantly uraninite mineralization. Ore bodies reach 27,000 m^2 in size and have 2 m in average thickness. The average grade is 0.6% U.

(Ad 3) Ore bodies in desilicified, albitized, and hematitized, commonly highly porous rocks occur adjacent to the individual brittle structures (Fig. 5b), and their shape usually follows the original metamorphic foliation of the host rocks. Disseminated coffinite is accompanied by less common uraninite and U-Zr-silicate. The ore bodies reach a maximum size of 30,000 m^2 with a grade of 0.10–0.15% U, exceptionally 0.3% U.

(Ad 4) Disseminated uranium mineralization bound to oblique fault zones is usually hosted by quartz-carbonate-sulfide breccias at intersections with diagonal and longitudinal structures. Compared to other types of mineralization, the ore bodies are small (1,000–5,000 m^2) but contain relatively high-grade ore (average grade 0.8% U, maximum 20% U in some ore shoots).

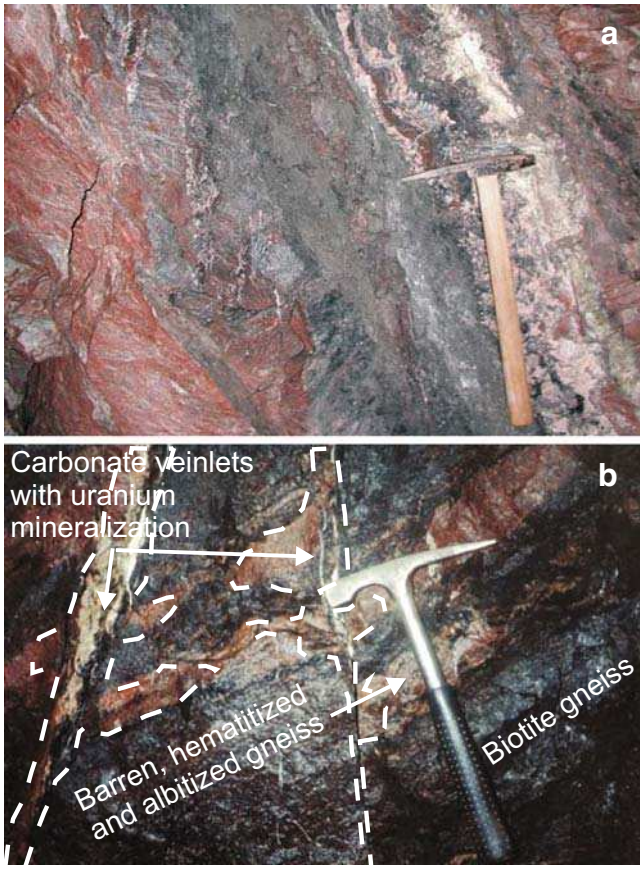


Fig. 5 Macroscopic documentation of ore mineralization and alteration at the Rožná deposit. **a** Chloritized and carbonatized fault cataclasite with disseminated uranium mineralization in pre-ore substage albitized and hematitized host gneiss. **b** Barren, pre-ore substage hematitized, albitized and desilicified biotite paragneiss with superimposed uranium mineralization in the proximity of younger carbonate veins. The extent of uranium mineralization is marked by *dashed line*

Materials and methods

Ore samples were collected from different levels and stopes of the Rožná I and Rožná II mines, mainly from levels 18–24 at depths of 900–1,200 m below surface or from the rock and mineral collection of both mines.

Thin sections and polished sections of rocks and ores were studied by polarized-light microscopy. Cathodoluminescence microscopy was performed on an optical microscope equipped with hot cathode HC2/LM (Simon-Neuser, Bochum, Germany).

Chemical compositions of rock-forming minerals were determined using the CamScan 3200 LINK ISIS microprobe (Czech Geological Survey, Prague), JEOL JXA-50 microprobe (Institute of Geology, Academy of Sciences of the Czech Republic), CAMECA SX-50 microprobe (Institute of Mineralogy, University of Hannover), and MICRO SPEC 2A electron microscope (Department of Mineralogy and Petrology, Masaryk University, Brno). Uranium mineralization was studied using the CamScan 4DV-LINK AN 10000 microprobe at the State Glass Institute, Hradec Králové.

XRD characteristics of clay minerals and their relative proportions in clay- and silt-size fractions were determined using a Philips PW 7310 diffractometer with CuK_{α} radiation and Ni filter standard set. Samples for XRD were prepared by hand crushing and rock disintegration in demineralized water using a sonic dismembrator for approximately 10–15 min. Clay (<2 μm) and fine silt (2–5 μm) fractions were then separated by sedimentation and centrifugation.

The ^{57}Fe Mössbauer spectra of the powderized chlorite and biotite samples were measured using ^{57}Co in Rh source in transmission geometry at room temperature. The velocity scale was calibrated against the spectrum of pure α-Fe foil. The analyses were carried out at the Institute of Material Physics, Brno.

Fluid inclusions were measured in siderite, calcite, quartz, and sphalerite of various paragenetic stages using a Chaixmeca heating–freezing stage (Poty et al. 1976) and a LINKAM THM combined heating- and freezing-stage, both under standard conditions. Salinity was determined after Bodnar and Vityk (1995), composition of the aqueous phase was evaluated after Borisenko (1977). P–V–T–X characteristics of H_2O–CO_2–CH_4 inclusions were evaluated after Bakker and Diamond (2000) and Van den Kerkhof and Thiery (2001).

Minerals for stable isotope determinations were separated by hand under the binocular microscope. SO_2 gas for sulfur isotope measurement was prepared from sulfides after Grinenko (1962). CO_2 gas from carbonates was prepared according to McCrea (1950). Quartz and silicate for oxygen isotope analyses were processed following the method of Clayton and Mayeda (1963). Measurement of carbon, oxygen, and sulfur isotope composition was done on a Finnigan MAT 251 IRMS at the Czech Geological Survey. The general reproducibility of $\delta^{13}C$ and $\delta^{18}O$ values of carbonates and $\delta^{34}S$ values of sulfides was ±0.1‰, and that of $\delta^{18}O$ values of quartz and silicates was ±0.2‰.

Samples for deuterium isotope (δD) determination were preheated in a ceramic oven to remove surface water and then heated in vacuo at 750°C. The released water was reduced over hot uranium metal and the resulting H_2 gas was collected on charcoal at −196°C. Isotopic analyses were performed on a Finnigan MAT 251 gas isotope ratio mass spectrometer. Data were corrected for $^3H^+$ production in the ion source and reported in the standard delta notation as per mil deviation from V-SMOW. External reproducibility is ±2.3‰ (1σ) based on repeat analyses of the Cambrian Formation Water Standard (CFW). The determinations were carried out by Actlabs Laboratories, Canada.

The extractable organic matter (EOM) of solid bitumen was extracted using a Soxhlet HT2 instrument (Tecator Company) and analyzed by gas chromatography–mass spectrometry. The extract was analyzed using a HP 5MS column (length 30 m, interior diameter 0.25 μm) in a Hewlett-Packard HP 5890 gas chromatogram with a flame ionization detector. The mass spectrometer (Hewlett-Packard 5985) source was at 220°C, using electron impact (70 eV) ionization, at 0.2 s per decade.

K–Ar age data were obtained from the <1-, <3-, and <5-μm separates of illite/white mica-rich samples. K–Ar dating was performed by Actlabs Laboratories, Canada. Data were stored and processed by a Hewlett-Packard MX-21-E data system. Details of the analytical procedures are given in Kapusta et al. (1997).

Chemical U–Pb dating on monazite was done using a JEOL JX 8600 microprobe equipped with four WDX spectrometers (Institute of Mineralogy, Salzburg University) and a CAMECA SX 100 microprobe (Dionýz Štúr Institute of Geology, Bratislava) using the method of Montel et al. (1996) and data processing after Ludwig (1980). The analytical error ranged between 0.04–0.05 wt% for Th, 0.025–0.030 wt% for U, and 0.010 wt% for Pb. Monazite samples with known concordant U–Pb ages (TIMS) were used as standards.

Stages and types of vein-style and disseminated mineralization

Vein-style and disseminated mineralization at Rožná comprises pre-uranium stage quartz-sulfide and carbonate-sulfide mineralization, uranium stage mineralization, and post-uranium quartz-carbonate-sulfide mineralization (Fig. 6). The relative time succession of individual mineralization stages is constrained by their textural relations.

Pre-uranium stage mineralization

The disseminated or veinlet-type quartz-sulfide mineralization of the pre-uranium stage is characterized by polygonal

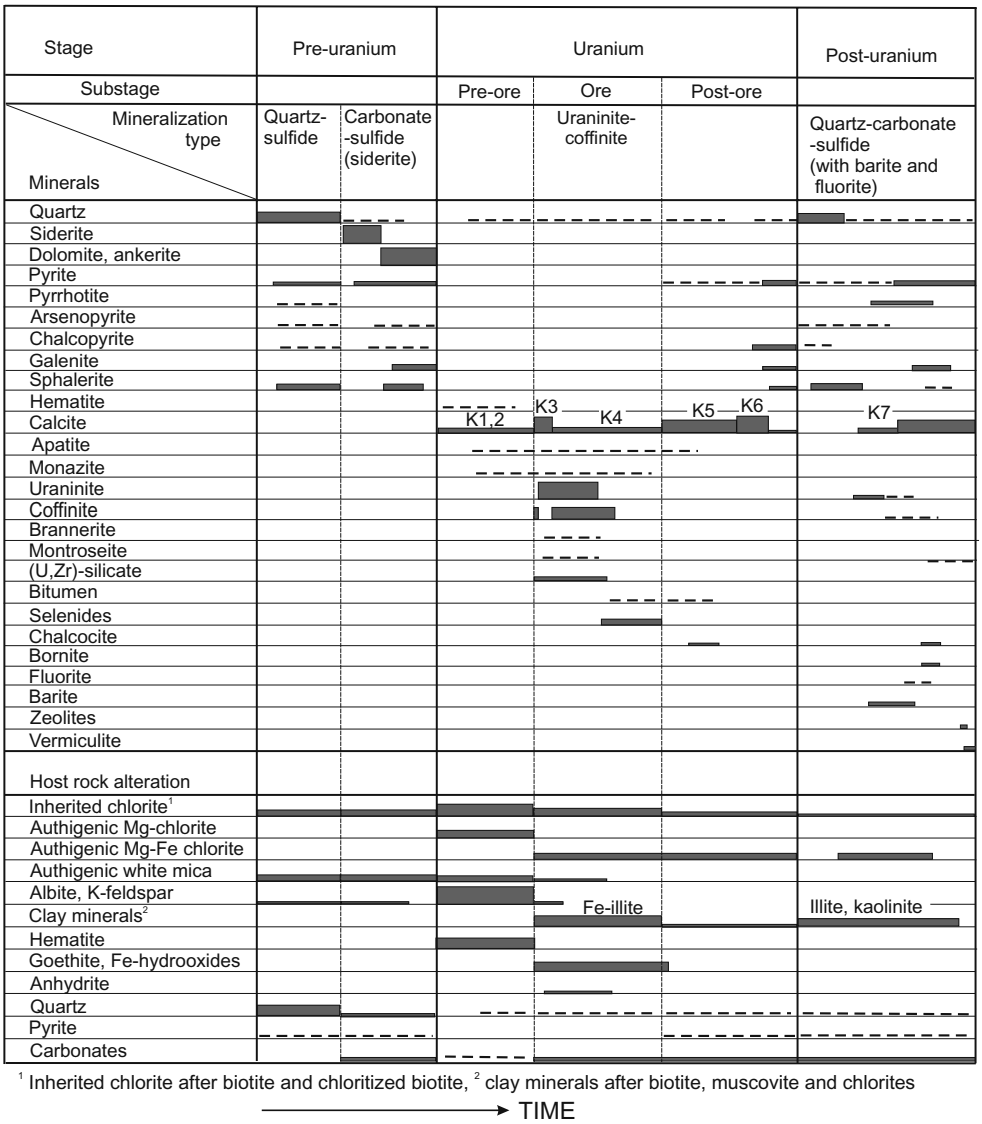


Fig. 6 Stages, substages and types of late Variscan and post-Variscan hydrothermal mineralization and stages of rock alteration at the Rožná deposit in relation to the individual mineralization types. Compiled after Arapov et al. (1984), Vilhelm et al. (1984), and the results of the present study

quartz, pyrrhotite, and xenomorphic pyrite with inclusions of chalcopyrite and arsenopyrite. Quartz is frequently replaced by siderite of the younger, vein-type carbonate-sulfide mineralization, which comprises siderite, ankerite-dolomite, galena, dark brown-colored sphalerite, and minor chalcopyrite, pyrite, tetrahedrite, boulangerite, and bournonite. Chalcopyrite is present in the form of xenomorphic aggregates or inclusions in sphalerite.

Uranium stage mineralization

The uranium stage can be schematically subdivided into the pre-ore, ore, and post-ore substages.

Pre-ore substage The pre-ore substage is characterized by widespread albitization, hematitization, chloritization, and carbonatization of metasedimentary rocks and migmatites. Veins and veinlets of K1 and K2 calcite commonly contain minute needle-shaped hematite and euhedral quartz grains.

Ore substage Uranium (and selenide) mineralization formed during the ore substage and comprises uraninite, coffinite, (U,Zr)-silicates, complex U–Ti–Si–Zr phases, and less important brannerite and montroseite. Generally, the coffinite to uraninite ratio increases with depth. At least two uraninite generations have been identified in calcite veins, in association with ore calcite (K3 and K4 calcite, Fig. 6). Aggregates of colloform, spherulitic, or irregularly shaped accumulations of uraninite are rimmed by slightly younger chlorite, minor comb-like quartz, and K5 calcite at some places. Almost all uraninite aggregates were replaced by coffinite to variable degree, as demonstrated by Si contents usually higher than 3.5 wt% in uraninite grains. In the disseminated uranium mineralization in cataclasites and

altered rocks, coffinite prevails over uraninite. Coffinite aggregates are distinctly microheterogeneous and contain remnants of original uraninite (Fig. 7a). The early generation of coffinite forms metamict, euhedral grains of micron size, partly replaced by a mixture of uranium oxides. In some polished sections, syntactic intergrowths of coffinite and newly formed zircon phases epitactically overgrowing older clastic zircon grains were observed (Fig. 7b). Variable Zr and U contents define a distinct zonal structure of euhedral grains. Late coffinite either replaces early coffinite and uraninite or forms irregular disseminations or larger accumulations in hydrothermally altered host rocks (Fig. 7c). Contraction cracks in late coffinite filled with younger carbonate are common. Both types of coffinite form disseminations along cleavage planes and margins of biotite, chloritized biotite (Fig. 7d) or chlorite, replace and rim corroded pyrite grains, or form, together with other uranium minerals, inclusions in bulbous-, lobate-, or cauliflower-shaped bitumen aggregates (Fig. 7e). Coffinite of both generations has variable Y (up to 10 wt% Y_2O_3) and Zr content (up to 12 wt% ZrO_2). The (U,Zr)-silicate forms distinct crystals up to 20 μm across (Fig. 7f), irregular aggregates or veinlets in altered host rock, or occurs as corroded fragments in bitumen. Its chemical composition varies between the chemical composition of zircon and coffinite end-members. Compared with coffinite, uraninite, and (U,Zr)-silicates, brannerite is far less common in uranium ores. In the process of alteration, the original brannerite was decomposed to form Ti-rich (over 90 wt% TiO_2) and more complex U–Ti–Si–Zr phases. All uranium minerals commonly rim corroded remnants of pre-uranium stage pyrite (Fig. 7g). Microheterogeneous, fine-grained to cryptocrystalline U–Ti–Si±Ca±Fe±Zr aggregates form irregularly distributed disseminations or replace metamorphic titanite (Fig. 7h). Uranium mineralization in some carbonate veins is accompanied by selenides. Generally, selenides are slightly younger than the main uranium mineralization as evidenced by local replacement of uraninite and coffinite by berzelianite in carbonate veins and by breccias of U-bearing carbonate clasts and hematitized rock fragments with uranium minerals cemented by fine-grained selenide-carbonate masses.

Post-ore substage The post-ore substage is formed by carbonates of several generations, chlorite, sulfides, and subordinate quartz. Cathodoluminescence images document that early generations of carbonates are commonly replaced by later generations (Fig. 8a,b), which makes the paragenetic interpretation and the interpretation of isotope composition of the carbonates difficult. Sulfide minerals are represented by minor pyrite, marcasite, galena, and sphalerite and by rare molybdenite, gersdorffite, nickeline, gudmundite, and siegenite.

Fig. 7 BSE images of uranium mineralization. **a** An example of uraninite coffinitization: coffinitized portions (*gray*) are microheterogeneous and contain relic uraninite (*white*). **b** A fully developed crystal of coffinite epitaxially overgrown on older zircon grain (*black*). Dark zones of coffinite, indicated by *arrows*, contain high amounts of $ZrSiO_4$. **c** Pseudomorphoses after coffinite I (*almost white*), formed mostly by uranium oxides. Uranium oxides are metasomatically replaced by coffinite II (*gray*). Coffinitized portions are of microheterogeneous nature. Replacement of older crystals proceeded not only from the outside but also along inner growth zones. Calcite (*black*) in the surroundings. **d** Uranium mineralization (coffinite and uraninite) developed along cleavage of chlorite (*ap* apatite). **e** A globule of uraniferous solid bitumen enclosing particles of coffinite, often with Zr admixture, uraninite-coffinite aggregates and locally also (Zr,U)-silicates. **f** Fully developed crystals of (U,Zr)-silicate (containing 38 wt% ZrO_2). **g** A well-developed crystal of pyrite (*gray*), replaced by Zr-coffinite (*white*). **h** Composite pseudomorph after titanite containing coffinite or uraninite (*white*) and Ti oxides (anatase or rutile)

Post-uranium stage mineralization

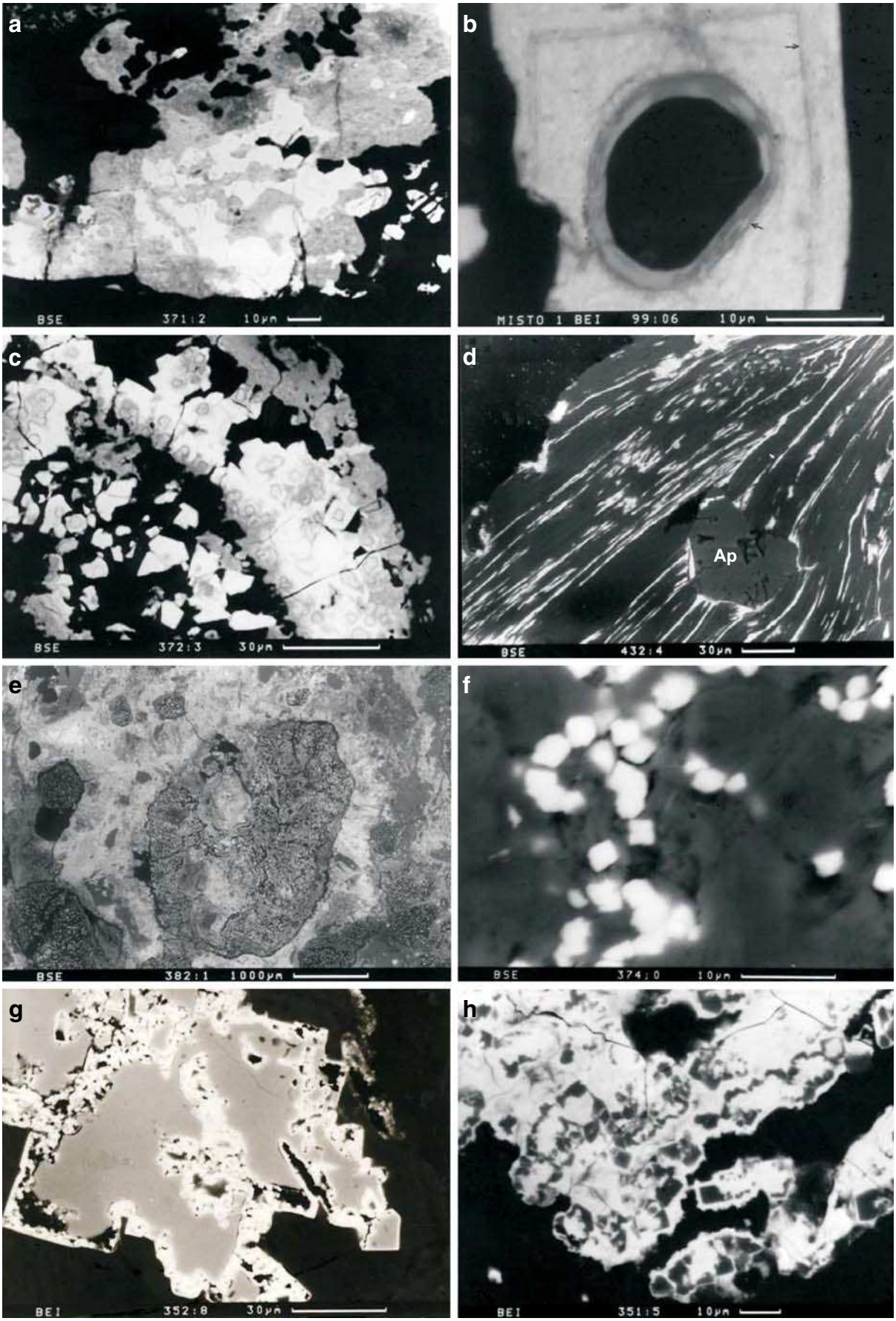
Quartz-carbonate-sulfide mineralization of the post-uranium stage forms either veins or veinlets that cut older uranium-bearing mineral assemblages or cements uraniferous carbonate breccias. The paragenetically oldest part of the mineralization is represented by quartz and yellow–brown-colored sphalerite followed by galena, and to a lesser extent by chalcocite, bournonite, tetrahedrite, freibergite, chalcopyrite, cubanite, arsenopyrite, dyscrasite, and native antimony enclosed in carbonate matrix. Tabular pyrrhotite and isometric pyrite are common. Gangue minerals are mainly quartz, carbonate (K7 calcite), barite, and minor chlorite and fluorite. In cathodoluminescence images, carbonate shows bright orange luminescence and distinct zonal structure (Fig. 8c). The paragenetically youngest part of the mineralization is represented by zeolites and vermiculite.

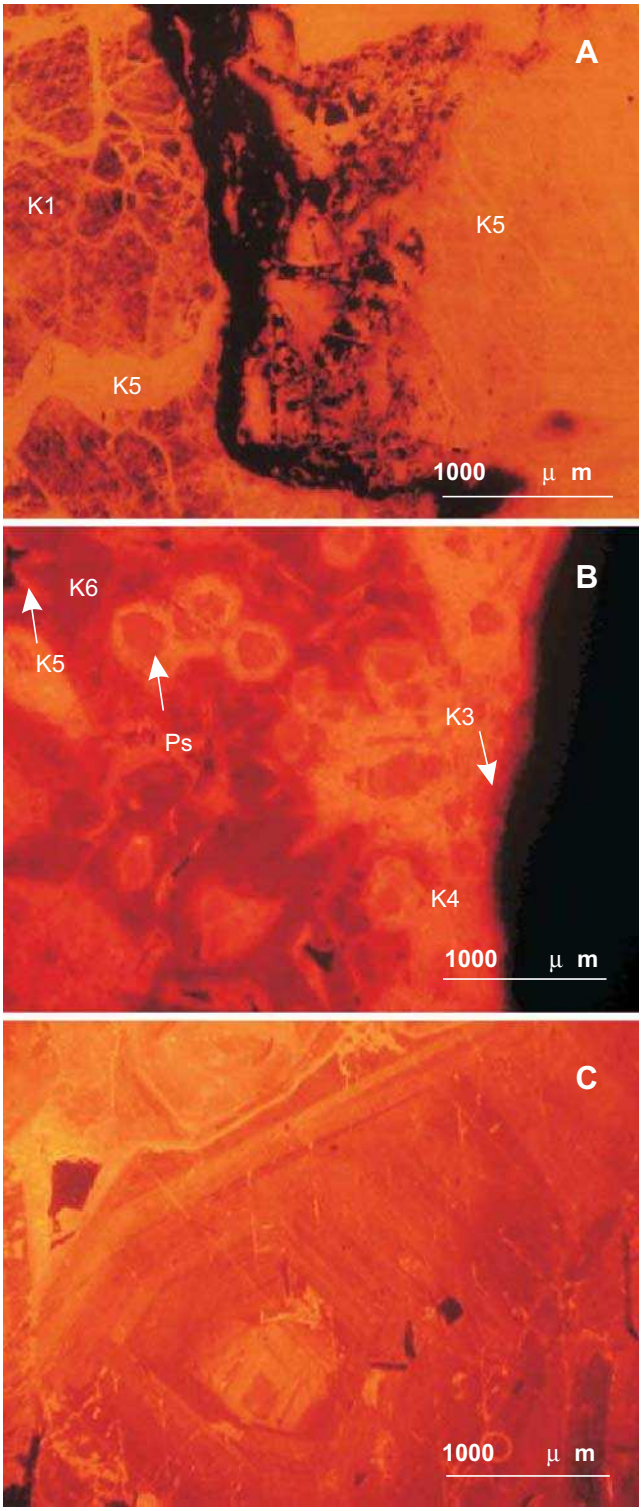
Petrology of retrograde-metamorphic and hydrothermal alteration styles

Large-scale host rock alteration styles at Rožná can be distinguished as (1) related to retrograde-metamorphic reactions in sheared host rocks and to the pre-uranium mineralization, (2) related to the pre-ore, ore, and post-ore substages of the uranium mineralization, and (3) alteration that accompanies quartz-carbonate-sulfide mineralization of the post-uranium stage (Fig. 6).

Retrograde-metamorphic and pre-uranium stage alteration

Rocks of the Rožná shear zone are—to a variable degree—affected by a greenschist-facies retrograde reequilibration of their amphibolite-facies mineral paragenesis, which is


a
BSE 371:2 10µm
b
MISTO 1 BEI 99:06 10µm
c
BSE 372:3 30µm
d
Ap
BSE 432:4 30µm
e
BSE 382:1 1000µm
f
BSE 374:0 10µm
g
BEI 352:8 30µm
h
BEI 351:5 10µm



◀ **Fig. 8** Cathodoluminescence photomicrographs of carbonates from the Rožná deposit. **a** Calcite of the pre-ore and post-ore substages of uranium mineralization. Pre-ore carbonate (K1) is replaced by post-ore carbonate (K5) which forms veinlets in the proximity of uranium mineralization (*black*) or replaces the pre-ore carbonate. The replacement is manifested by the presence of "ghost" structures, i.e., minute hematite, silicate and quartz inclusions in the original carbonate. **b** Ore substage calcite forms a very thin zone with dark red CL color (K3), lining an accumulation of uraninite (*black*). This zone is overgrown by younger post-ore carbonate (K4) with bright red luminescence, followed by younger carbonate showing dark red luminescence (K5). The youngest carbonate (K6) shows dull orange luminescence. Polygonal, in places frequently hexagonal objects with prominent internal structure (Ps) probably represent pseudomorphs of post-ore K5 or K6 calcite after quartz. **c** Post-uranium stage quartz-carbonate-sulfide mineralization. Calcite crystals show frequent oscillatory zoning, documenting rapid changes in physicochemical conditions

characterized by decomposition of plagioclase, formation of white mica, Ca silicates (zoisite, epidote), and albite. K-feldspar grains are fractured and exhibit strong undulatory extinction. Quartz shows recrystallization, subgrain rotation, and local remobilization; biotite and garnet are affected by chloritization and sericitization. Transformation of biotite to protochlorite (K_2O>0.3 wt%; Deer et al. 1964) is manifested by a gradual decrease in the K_2O content from 8.9–7.0 wt% in biotite to 5.5–0.6 wt% in chloritized biotite. The SiO_2 content decreases from 38.2–37.2 wt% (slightly chloritized biotite) to 35.6–30.2 wt% (chloritized biotite, Fig. 9, Table 1, analyses 1 and 2). The Al_2O_3 and MgO contents in chloritized biotite are comparable to those in original biotite; the FeO content, however, increases from 11.9–12.9 wt% (biotite) to 14.3–22.3 wt% (chloritized biotite and protochlorite). In inherited chlorite, the content of SiO_2 further decreases and FeO contents increase to 20.5–29.6 wt% (Table 1, analysis 3). The content of MgO in inherited chlorites is lower when compared with chloritized biotite and protochlorite and varies between 6.0 and 18.9 wt%. Inherited chlorites either preserve the morphology of the metamorphic biotite or form fluidal, fine-grained aggregates in cataclasites (matrix chlorite). Alteration associated with pre-uranium stage mineralization is similar to the retrograde-metamorphic alteration along nonmineralized shear zones with the exception of the strong silicification and and/or carbonatization of wall rocks.

Uranium stage alteration

Pre-ore substage In contrast to the alteration associated with pre-uranium mineralization dominated by white mica, slightly chloritized biotite, inherited chlorite, and pyrite, the pre-ore substage alteration (Fig. 6) is characterized by widespread hematitization and albitization of the host rock (Fig. 10a,b). The altered rocks usually form tabular bodies up to 250×50 m in size adjacent to fault zones and occur mostly in deeper parts of the deposit. In places, zones of pre-ore altered rocks are cut and displaced along younger, uraninite- and coffinite-bearing brittle structures. The original plagioclase ($An_{20–30}$) in pre-ore altered rocks is almost entirely replaced by albite ($An_{0–5}$) and, in addition,

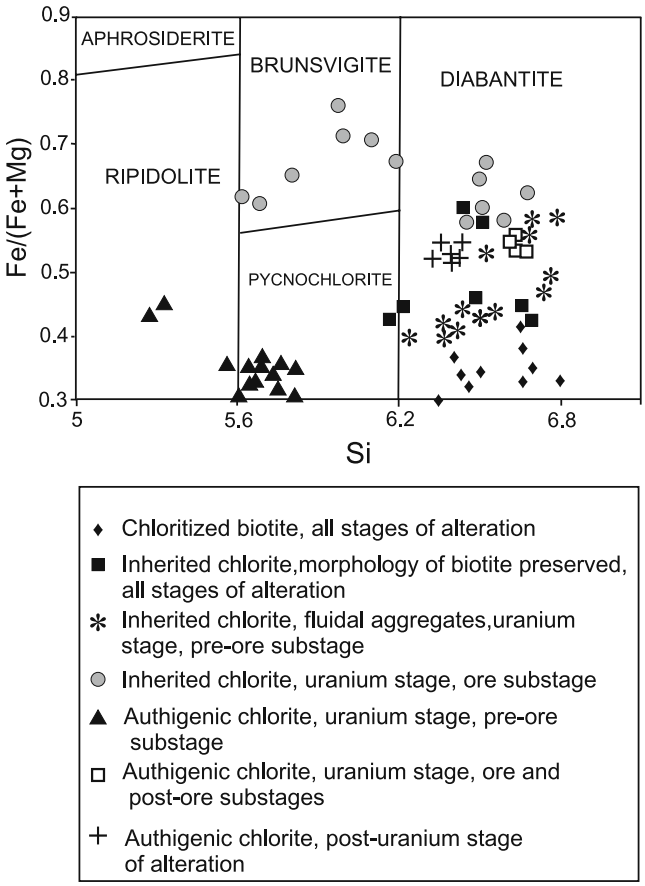


Fig. 9 Fe/(Fe+Mg) vs. Si ratio in chloritized biotite, inherited and authigenic chlorite at Rožná. Note high iron contents in inherited chlorite close to uranium mineralization. Boundaries of individual phases after Hey (1954)

minor authigenic, lath-shaped albite is formed. A very small amount of K-feldspar (adularia) is found in some samples. The chemical composition of chloritized biotite, protochlorite, and inherited chlorite in hematitized and albitized rocks is generally very similar to that of retrograde-metamorphic chlorite. However, as revealed by the results of Mössbauer spectroscopy, the Fe^{3+}/Fe^{2+} ratio in chloritized biotite and protochlorite in albitized and hematitized rocks is higher (0.075 to 0.111) when compared to chloritized biotite from retrograde-metamorphosed rocks (0.041). Besides inherited chlorites, fan-like aggregates of authigenic Mg chlorite (pycnochlorite) up to several millimeters across occur in peripheral parts of the pre-ore alteration halo (Fig. 10c,d). The authigenic chlorite is characterized by a low Fe/(Fe+Mg) ratio and a low Si content (Fig. 9, Table 1, analysis 6). Authigenic chlorite data were used to calculate the temperature of alteration. Their crystal chemistry indicates temperatures ranging from 260°C to 310°C, depending on the thermometer used (Table 2). In the classification diagram of dioctahedral micas (Rieder et al. 1998, Fig. 11), pre-ore substage white mica plots in the field of muscovite. The $^{vi}R^{II}/(^{vi}R^{II}+^{vi}R^{III})$ ratio is low (<0.05), and the $^{vi}Al/(^{vi}Al+^{vi}Fe^{III})$ ratio is <0.9. The interplanar positions are almost entirely saturated by cations (1.7 to 2.0, calculated on the basis of 20 O). Pre-ore substage muscovite is characterized by elevated Na contents (0.1 to 0.4) and by a low degree of hydration (Table 3, analyses 1 and 2).

Ore substage The hydrothermal alteration of the ore substage overlaps with the pre-ore substage alteration in time and space, but is generally confined to the vicinity of the uranium ore bodies. In the peripheral part of the ore substage alteration halo, which extends up to 80 m from the ore bodies, biotite, previously altered biotite, and inherited chlorite are transformed to Fe-rich [Fe/(Fe+Mg)=0.6–0.8] chlorite (Fig. 9, Table 1, analysis 5). As revealed by Mössbauer spectroscopy, the Fe^{3+}/Fe^{2+} ratio in inherited chlorite is high (0.087), which points to the oxidative character of the ore fluids. In the inner part of the halo, adjacent to and within high-grade uranium ore bodies, Fe-rich chlorite is almost entirely decomposed into a mixture of XRD-amorphous hydrooxides of iron and Fe-rich illite (Fig. 10e). Illite from the ore substage alteration halo differs from the pre-ore substage muscovite in its low cation content in interlayer positions (1.1–1.2) and in higher $^{vi}R^{II}/(^{vi}R^{II}+^{vi}R^{III})$ and $^{vi}Al/(^{vi}Al+^{vi}Fe^{III})$ ratios (0.04–0.06 and 0.35–0.8, respectively), calculated on the basis of 20 O (Fig. 11, Table 3, analyses 3 and 4). The Fe_2O_3 content ranges between 4.5 and 10.5 wt%. Anhydrite commonly occurs in association with Fe-rich illite and iron hydrooxides. Minor authigenic chlorite that overgrows uraninite and coffinite in carbonate veins is characterized by higher Fe/(Fe+Mg) ratios (0.5–0.6) compared to those of pre-ore substage authigenic Mg-rich chlorite. Authigenic apatite and monazite form accessories in ore stage hydrothermally altered rocks.

Post-ore substage Compared with the voluminous pre-ore and syn-ore substage alteration, post-ore substage alteration is restricted to small authigenic chlorite-carbonate veins and veinlets (Fig. 10f) and disseminations of chlorite and pyrite in carbonatized host rocks. The chemical composition of authigenic chlorite in carbonate veins is comparable with the chemistry of ore substage authigenic chlorite and its chemistry indicates temperatures ranging from 150°C to 170°C, depending on the thermometer used (Table 2).

Post-uranium stage alteration

Alteration styles that accompany post-uranium quartz-carbonate-sulfide mineralization comprise carbonatization, silicification, and argillization of the host rock. The clay mineral assemblage is dominated by illite with minor

Table 1 Representative composition of chloritized biotite, inherited chlorite, and authigenic chlorite at the Rožná deposit

Analysis no.	1	2	3	4	5	6	7	8
Sample no.	ZA-30/1	ZA-35/25	SuPo-3/11	Me5/47	MzB2/9	ZA10/5	ZA-30/17	SP-10/10
Na_2O (%)	0.62	0.68	0.0	0.0	0.0	0.69	0.85	0.34
MgO (%)	17.40	17.37	15.41	13.95	6.60	21.37	14.19	10.78
Al_2O_3 (%)	14.66	15.66	18.11	13.21	18.11	20.47	13.18	16.50
SiO_2 (%)	38.20	35.56	28.67	30.71	26.82	28.71	31.46	30.54
K_2O (%)	8.90	5.45	0.47	0.39	0.0	0.07	0.03	0.0
CaO (%)	0.08	0.08	0.0	0.28	0.26	0.05	0.29	0.41
TiO_2 (%)	2.56	3.02	0.18	0.0	0.17	0.11	0.0	0.18
Cr_2O_3 (%)	0.09	0.09	0.0	0.0	0.0	0.10	0.13	0.0
MnO (%)	0.49	0.14	0.26	0.39	0.22	0.38	0.09	0.17
FeO (%)	11.93	15.12	20.57	29.61	35.55	17.99	29.44	24.63
Σ	94.76	92.83	83.63	88.15	87.95	89.83	89.44	83.97
Structural formulae based on 28 oxygen atoms								
Si	7.19	6.81	6.61	6.57	5.96	5.67	6.61	6.63
Al(IV)	0.81	1.19	1.84	1.43	2.04	2.33	1.39	1.37
Al(VI)	2.44	2.34	2.75	1.89	2.71	2.44	1.87	2.96
Ti	0.36	0.43	0.03	0.0	0.0	0.02	0.0	0.0
Fe	1.88	2.42	3.70	5.29	6.61	2.97	5.17	4.47
Mn	0.08	0.02	0.05	0.07	0.04	0.06	0.02	0.03
Mg	4.88	4.96	4.94	4.45	2.19	6.29	4.44	3.60
Ca	0.02	0.02	0.0	0.06	0.06	0.01	0.07	0.08
Na	0.23	0.25	0.0	0.0	0.0	0.0	0.36	0.0
K	2.14	1.33	0.13	0.0	0.0	0.0	0.0	0.0

Analysis 1: slightly chloritized biotite, pre-uranium stage, *analysis 2*: chloritized biotite, pre-uranium stage, *analysis 3*: inherited chlorite, morphology of the original biotite preserved, pre-uranium stage, *analysis 4*: inherited matrix chlorite, uranium stage, pre-ore substage, *analysis 5*: Fe-rich, inherited matrix chlorite, uranium stage, ore substage, *analysis 6*: authigenic, fan-like chlorite, uranium stage, pre-ore substage, *analysis 7*: authigenic chlorite, uranium stage, ore substage, *analysis 8*: authigenic, fan-like chlorite, post-uranium stage

kaolinite and chlorite. No mixed layers and smectite group minerals were detected in the <2-μm fraction. Compared with illite that accompanies uranium mineralization, illite from post-uranium alteration has lower Fe^{3+} content [$^{vi}Al/(^{vi}Al+^{vi}Fe^{III})$=0.35–0.80] and more variable K content in interlayer positions (1.11–1.65, Fig. 11, Table 3, analyses 5 and 6). In contrast to relatively Na-rich uranium-related muscovite and illite, Na contents in post-uranium illite are low. Rare authigenic post-uranium stage chlorite (Fig. 9, Table 1, analysis 8) forms fan-like, light green aggregates, locally replacing fluorite. The temperature of its formation was estimated at 170°C to 190°C (Table 2).

Fluid inclusions

Retrograde-metamorphic fluids and fluids from pre-uranium mineralization

Primary inclusions of H_2O and CO_2–CH_4 and inclusions of mixtures of these phases were found in quartz of the retrograde-metamorphosed quartz-muscovite veins. H_2O inclusions have low salinities (0.7–2.1 wt% NaCl eq; Fig. 12a). Temperatures of melting of CO_2 (T_m CO_2) in the CO_2–CH_4 inclusions range between −58.1°C and −59.4°C, and the proportion of CH_4 in these inclusions is 8–16 mol%. Temperatures of homogenization of CO_2 into the liquid phase (T_h $CO_{2(L)}$) range between −1.8°C and 22.0°C, which corresponds to a density of 0.750–0.940 g/cm^3. T_m CO_2 in the H_2O–CO_2–CH_4 inclusions range between −58.8°C and −59.4°C, and the proportion of gaseous CH_4 is 20–22 mol%. CO_2 in these inclusions homogenized to vapor at 8.9–9.9°C, which corresponds to the density of 0.130–0.134 g/cm^3. Temperatures of melting of CO_2 clathrate (T_m clat CO_2) range between 9.8°C and 9.9°C, which corresponds to salinities of approximately 1 wt% NaCl eq.

In early barren quartz of quartz-sulfide veins, only secondary H_2O–CO_2–CH_4 and CO_2–CH_4 inclusions were found. These inclusions are characterized by T_m CO_2 of −59.1°C to −59.3°C, which indicates XCH_4 in gaseous phase from 0.14 to 0.15. The T_h $CO_{2(L)}$ range between 17.6°C and 26.0°C, which corresponds to a density of the gaseous phase between 0.697 and 0.802 g/cm^3. T_m clat CO_2 range between 7.6°C and 9.2°C, which corresponds to salinities of 1.5–4.5 wt% NaCl eq. (Fig. 12a). Several types of primary inclusions were found in late quartz in quartz-

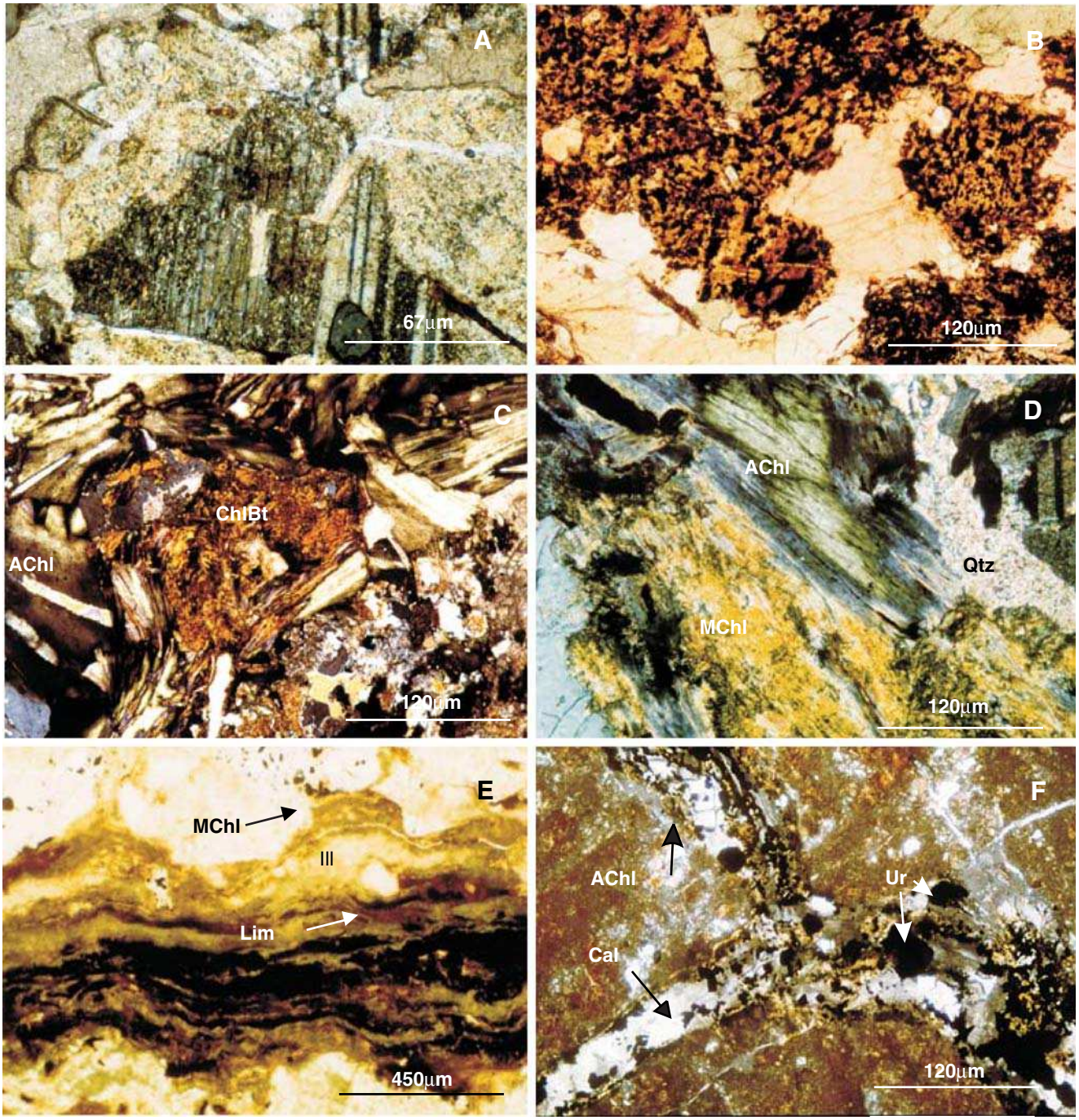


Fig. 10 Photomicrographs of hydrothermal alteration related to uranium mineralization at Rožná. **a** Relict of plagioclase enclosed in albitized and hematitized rocks of the pre-ore substage of uranium mineralization. Transmitted light, crossed nicols. **b** Hydrothermal alteration of the pre-ore substage of U mineralization. The original rock (biotite gneiss) is completely replaced by albite, hematite (*brown*) and white mica (*colorless* laths). Transmitted plane light. **c** Chloritized biotite (ChlB) and newly formed magnesian chlorite (AChl) in hydrothermally altered gneiss. Pre-ore substage of uranium mineralization. Transmitted light, crossed nicols. **d** Albitized and chloritized biotite gneiss with corroded quartz grains. Biotite is completely chloritized, giving rise to matrix chlorite (MChl). Besides matrix chlorite, the rock also contains platy laths of authigenic chlorite (AChl) of pycnochlorite composition. Pre-ore substage of uranium mineralization. **e** Uranium mineralization (*black*) rimmed by a mixture of hydrooxides of iron (Lim), Fe-rich illite (Ill) and remnants of pre-ore, Fe-rich matrix chlorite (MChl). Ore substage of mineralization. **f** Calcite veinlets (Ca) with uraninite (Ur) and authigenic post-ore chlorite (AChl) in limonitized and argillized cataclasite. Post-ore substage of uranium mineralization. Transmitted plane light

Table 2 Temperatures of formation of authigenic chlorite calculated on the basis of its chemical composition after different authors

	Cathelineau and Neiva (1985)	Cathelineau (1988)	Jowett (1991)	Zang and Fyfe (1995)
Pre-ore substage chlorite (n=12), °C	259–278 (263)	334–295 (311)	288–335 (311)	251–277 (263)
Post-ore substage chlorite (n=4), °C	163–165 (164)	159–161 (160)	167–170 (168)	143–147 (145)
Post-uranium stage chlorite (n=6), °C	183–196 (184)	189–208 (190)	167–215 (198)	164–179 (165)

Mean value is given in parentheses.
n: number of analyzed samples

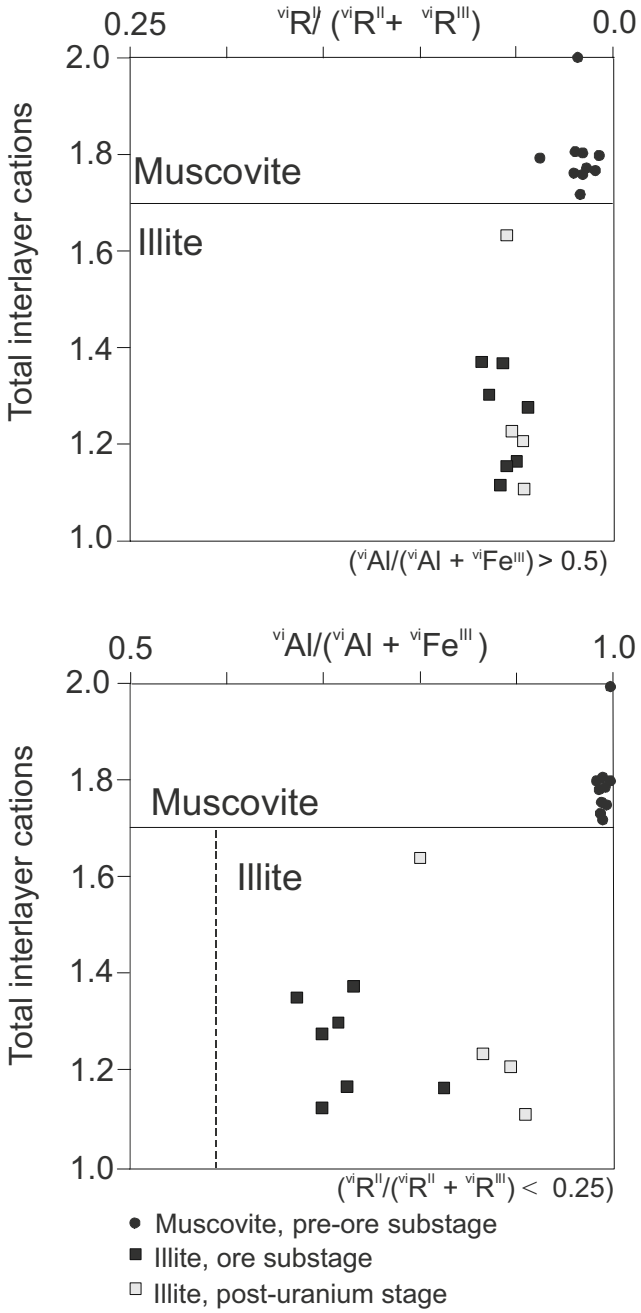


Fig. 11 Chemical analyses of pre-ore substage muscovite, ore substage illite and post-uranium stage illite plotted in the classification diagram of dioctahedral micas after Rieder et al. (1998). Recalculated to 20 oxygen atoms

sulfide veins, which host pyrrhotite, pyrite, sphalerite, and chalcopyrite mineralization. Primary H_2O–CO_2–CH_4 and CO_2–CH_4 inclusions have variable liquid to vapor ratios (LVR). T_m CO_2 range from −58.1°C to −59.4°C, and XCH_4 in the gaseous phase is 0.08–0.16. T_h $CO_{2(L)}$ range between −1.8°C and 22.4°C, which indicates CO_2 densities of 0.749–0.940 g/cm^3. In several H_2O–CO_2–CH_4 inclusions, CO_2 homogenized to the gaseous phase at temperatures of 8.9–9.9°C (DCO_2=0.130–0.134 g/cm^3). In these inclusions, T_m CO_2 range from −59.2°C to −59.4°C, thus XCH_4 in the gaseous phase is approximately 0.22. T_m clat CO_2, measured in only one inclusion, is 9.8°C, indicating a low salinity of about 1 wt% NaCl eq. The variable LVRs in H_2O–CO_2–CH_4 inclusions indicate that they were trapped in a heterogeneous environment under conditions of partial immiscibility of a H_2O-rich and a CO_2±CH_4-rich phase. Low salinities of the aqueous solution (approximately 3 wt%) imply complete miscibility of the aqueous and gaseous phases at 300°C (Hendel and Hollister 1981). The irregular LVRs of the studied inclusions suggest that these were trapped at temperatures close to or lower than 300°C. Only few primary CH_4 inclusions were found in some quartz grains. Their T_h $CH_{4(L)}$ are between −95.7°C and −98.8°C, which corresponds to DCH_4 of 0.28–0.30 g/cm^3. In rare secondary CH_4 inclusions, CH_4 homogenized to liquid at temperatures between −119.8°C and −129°C, indicating DCH_4 of 0.35–0.37 g/cm^3. Temperatures of melting of ice of primary H_2O-only fluid inclusions range from −0.4°C to −1.2°C, which corresponds to low fluid salinities (0.7–2.1 wt% NaCl eq).

Fluids from uranium mineralization

Pre-ore substage Dominantly aqueous inclusions and, to a lesser extent, CH_4, CO_2–CH_4, and H_2O–CO_2–CH_4 inclusions were observed in quartz of the pre-ore substage. Homogenization temperatures (T_h) of the primary H_2O inclusions in quartz and K1 to K2 carbonates (Fig. 6) range between 119°C and 206°C, and salinities between 7.3 and 21.8 wt% NaCl eq (temperatures of final ice melting T_m= −4.6°C to −19.1°C; Fig. 12a). Temperatures of first ice melting (T_{fm}) range between −52°C and −54°C, thus indicating a high content of $CaCl_2$ and probably also

Table 3 Representative chemical analyses of muscovite and illite from the Rožná deposit

Analysis no.	1	2	3	4	5	6
Sample no.	ALT2/12	ALT6/15	M6/21	M6/25	M5/1	SPO/2
SiO_2 (%)	48.82	47.9	43.96	44.93	47.17	48.52
TiO_2 (%)	0.0	0.0	0.49	0.52	0.11	0.08
Al_2O_3 (%)	34.37	33.59	22.46	23.46	30.94	26.03
Fe_2O_3 (%)	0.22	0.57	10.09	9.42	3.44	6.22
FeO (%)	0.04	0.09	1.48	1.38	0.56	1.02
MnO (%)	0.0	0.16	0.0	0.02	0.04	0.04
MgO (%)	0.56	0.45	1.47	1.40	1.60	1.78
CaO (%)	0.0	0.0	0.33	0.21	0.22	0.15
Na_2O (%)	0.40	0.48	0.62	0.65	0.08	0.06
K_2O (%)	9.69	9.71	4.65	5.05	6.32	9.31
Σ	94.10	94.39	85.55	87.04	90.15	93.00
Structural formulae, occupancy and charge, based on 20 oxygen atoms (after Stevens 1946)						
Tetrahedral sheet						
Si	6.47	6.44	6.57	6.59	6.49	6.69
Al	1.53	1.55	1.37	1.36	1.51	1.31
Ti	0.0	0.01	0.06	0.06	0.01	0.01
Occupancy	8	8	8	8	8	8
Charge	30.47	30.45	30.63	30.64	30.00	30.69
Octahedral sheet						
Al(III)	3.83	3.81	2.59	2.70	3.51	2.92
Fe(II)	0.01	0.01	0.19	0.17	0.06	0.12
Fe(III)	0.02	0.04	1.14	1.04	0.36	0.65
Mn(II)	0.0	0.02	0.0	0.0	0.01	0.01
Mg(II)	0.11	0.09	0.33	0.31	0.33	0.37
Occupancy	3.97	3.97	4.24	4.21	4.26	4.05
Charge	11.79	11.79	12.20	12.16	12.40	11.67
Interlayer sheet						
Ca	0.0	0.0	0.05	0.03	0.0	0.0
Na	0.10	0.13	0.18	0.19	0.0	0.0
K	1.64	1.63	0.89	0.94	1.11	1.64
Occupancy	1.74	1.76	1.12	1.16	1.11	1.64
Charge	1.74	1.76	1.17	1.20	1.11	1.64

Analyses 1 and 2: muscovite, uranium stage, pre-ore substage, *analyses 3 and 4*: Fe-illite, uranium stage, ore substage, *analyses 5 and 6*: illite, post-uranium stage.

$MgCl_2$ or $FeCl_2$ in the solution (Fig. 12b). T_h were measured in only one sample with inclusions with uniform LVRs and ranged between 181°C and 206°C. For other inclusions, T_h estimation was prevented by variable LVRs. Primary H_2O–CO_2–CH_4 inclusions with variable LVRs were found in some quartz crystals. These inclusions display T_m CO_2 of −59.3°C to −59.5°C, thus XCH_4 in the gaseous phase is 0.33–0.35. T_h CO_2 to vapor vary from −5.5°C to −7.5°C (DCO_2=0.076–0.080 g/cm^3). The salinity of the aqueous solution is approximately 7.5 wt% NaCl eq (T_m clat CO_2=5.4–5.6°C).

Ore substage Primary H_2O inclusions with variable LVRs occur in K3 and K4 ore substage carbonate (Fig. 6). Homogenization temperatures for inclusions with a consistent LVR (0.9) are 152–174°C. The salinities are highly variable (Fig. 12a) and range from 3.1 to 23.1 wt% NaCl eq (T_m=−1.8°C to −21.0°C). T_{fm} range from −52°C to −54.2°C and indicate high $CaCl_2$ concentrations in the solution (Fig. 12b).

Post-ore substage Primary aqueous inclusions in post-ore substage K5 and K6 carbonate (Fig. 6) and in associated quartz show variable LVRs. Few inclusions with LVRs of approximately 0.9 display T_h of 84–128°C. Salinities of aqueous solutions in calcite and quartz range from 0.5 to 12.4 wt% NaCl eq (T_m=−0.3°C to −8.6°C), and T_{fm} between −35°C and −41°C (Fig. 12a,b). The given range of T_{fm} values cannot be interpreted unambiguously. The probable components of the aqueous solution are NaCl,

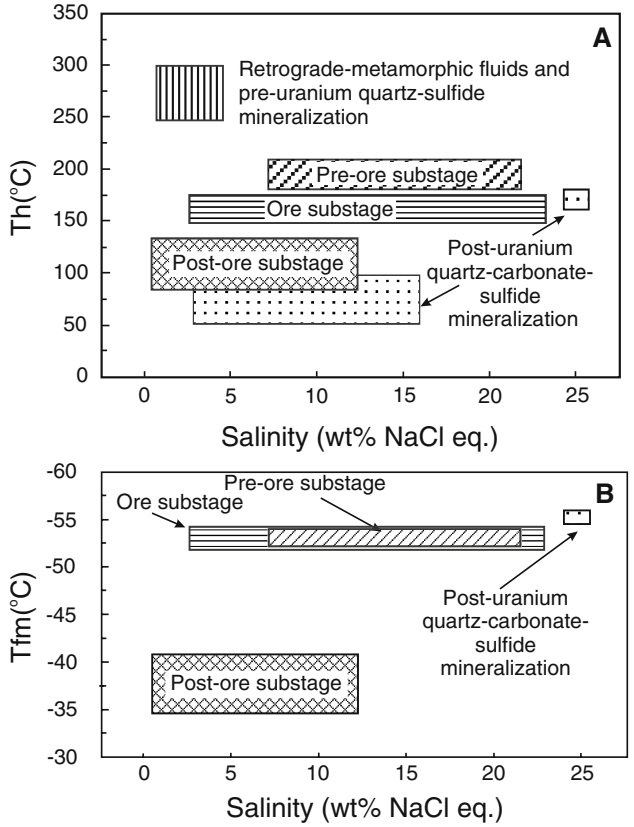


Fig. 12 Homogenization temperatures vs. salinities (**a**), and temperature of the first melting vs. salinity (**b**) of fluid inclusions in minerals of the pre-uranium stage carbonate-sulfide mineralization, pre-ore, ore and post-ore substages of uranium mineralization and of the post-uranium stage quartz-carbonate-sulfide mineralization

$MgCl_2$, $FeCl_2$, and KCl (Borisenko 1977). Moreover, coexisting primary H_2O, CH_4, or H_2O–CH_4 inclusions with variable LVRs are exceptionally found in quartz that forms a part of the chlorite-pyrite-calcite-bitumen post-ore substage mineral association. The inclusions are believed to be trapped under conditions of H_2O and CH_4 immiscibility. T_h of H_2O-only inclusions are 118–131°C and salinities are 8–9 wt% NaCl eq. T_h of CH_4 to the gaseous phase (−85.2°C to −872°C) indicate its low density (0.081–0.094 g/cm^3).

Fluids from post-uranium mineralization

The fluid inclusion characteristics of this stage are highly variable. Early quartz in association with sphalerite contains primary aqueous inclusions with LVRs of approximately 0.9 with T_h of 165–178°C and high salinities (25.0–25.5 wt% NaCl eq, Fig. 12a). In paragenetically younger minerals, the salinities of aqueous solutions range between 3.2–16.3 wt% NaCl eq in quartz, 3.9–11.8 wt% NaCl eq in calcite, and 4.5–8.7 wt% NaCl eq in barite. The T_{fm} value of −56.2°C in barite-hosted inclusions (Fig. 12b) indicates $CaCl_2$–NaCl–H_2O composition of the solution. In drusy quartz, monophase liquid-only inclusions are found, indicating low temperatures (<100°C) of the latest stage of fluid activity.

Geochemistry of stable isotopes

Sulfur

At Rožná, sulfides occur either as stratabound pyrite and pyrrhotite disseminations in host gneiss, marble and in metamorphosed barite-hyalophane-sulfide and anhydrite-pyrite mineralization (Kříbek et al. 2002) or form a part of pre-uranium quartz-sulfide, carbonate-sulfide, and post-uranium quartz-carbonate-sulfide mineralization (Fig. 13). The amount of sulfides accompanying the uranium mineralization is negligible.

Generally positive $\delta^{34}S$ values of metamorphosed (pre-Variscan) stratabound sulfides reflect the isotope composition of sulfate sulfur of marine origin (Kříbek et al. 1996, 2002). The isotope composition of pre-uranium stage quartz-sulfide mineralization ($\delta^{34}S$=−5 to +28‰, CDT) thus reflects a host rock source of sulfur. The pre-uranium stage carbonate-sulfide mineralization (Fig. 6), however, has a narrow compositional range between −3‰ and +4‰ (CDT), and the calculated $\delta^{34}S$ value of the fluid phase close to 0‰ points to a homogeneous, lower crustal source of sulfur (Fig. 13).

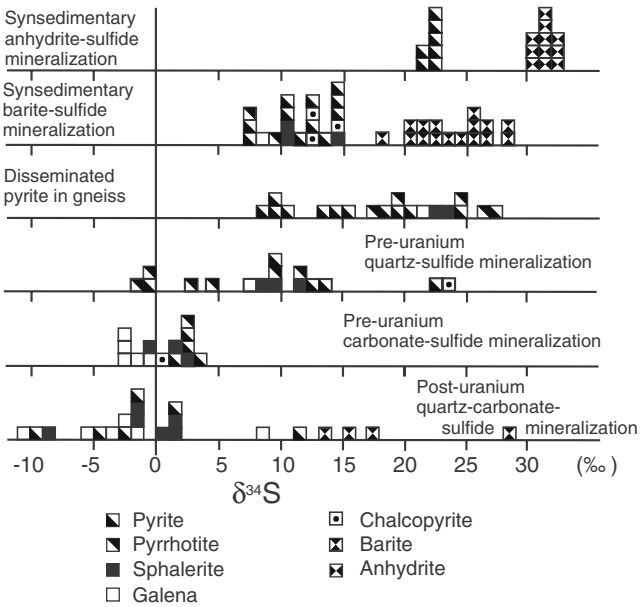


Fig. 13 Histogram of isotope composition data on sulfide and sulfate sulfur from the area of the Rožná uranium deposit, sorted by types and stages of mineralization. Data taken from Vencelides (1991), Kříbek et al. (1996, 2002), and new data

Sulfides formed during the post-uranium stage quartz-carbonate-sulfide mineralization show variable $\delta^{34}S$ values and a large fractionation between sulfide and sulfate (barite) (Fig. 13). Sulfide thermometry based on the sphalerite–galena pair suggests temperatures close to 300°C for the pre-uranium stage mineralization and 200°C to 100°C for the post-uranium stage mineralization (Fig. 14).

Carbon and oxygen

Carbonates of the pre-uranium stage carbonate-sulfide mineralization have $\delta^{13}C$ values between −10‰ and −6.3‰ (PDB, Fig. 15). The calculated isotope compositions of CO_2 (or H_2CO_3) for temperatures of about 300°C range between −9‰ and −11‰ (temperature estimated according to sulfide thermometry). Low $\delta^{13}C$ values in some samples indicate that the carbonate carbon is derived from multiple sources including CO_2 produced by hydrolysis of graphite in the source area.

The $\delta^{13}C$ values of pre-ore substage K1 and K2 carbonates and ore substage K3 and K4 carbonates of the uranium mineralization are very homogeneous ($\delta^{13}C$=−3‰ to −7‰), and their composition corresponds to a deep-seated origin of carbon. A recalculation to fluid $\delta^{13}C$ values is complicated by the fact that the H_2CO_3/HCO_3^- ratio is not precisely known and probably varied during the low-temperature stages. A $\delta^{13}C$ range of −4‰ to −8‰ can be estimated for the temperature of the main phase of the uranium deposition (approximately 150°C, based on fluid inclusion studies).

Compared with ore carbonates, calcites of the post-ore substage of the uranium mineralization stage (calcite K5 and K6) and carbonates of quartz-carbonate-sulfide mineralization of the post-uranium stage (calcite K7) are characterized by more variable $\delta^{13}C$ values (Fig. 15), thus indicating multiple sources of carbon including host rock carbonates and percolating meteoric waters. In contrast to the relatively homogeneous oxygen isotope composition of early generations of K1 to K4 carbonate ($\delta^{18}O$=+13‰ to +18‰ SMOW), the $\delta^{18}O$ values of the late generations K5 to K7 are more variable (+4‰ to +17‰), thus indicating multiple sources of solutions, including meteoric waters.

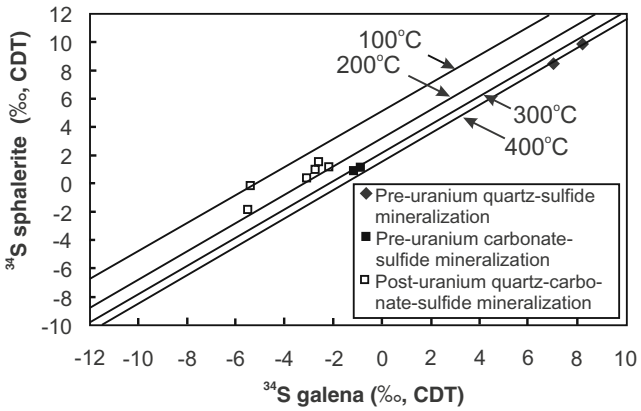


Fig. 14 Sphalerite–galena pairs of pre-uranium and post-uranium sulfide mineralizations. Isotherms are calculated on the basis of the formula of Ohmoto and Rye (1979)

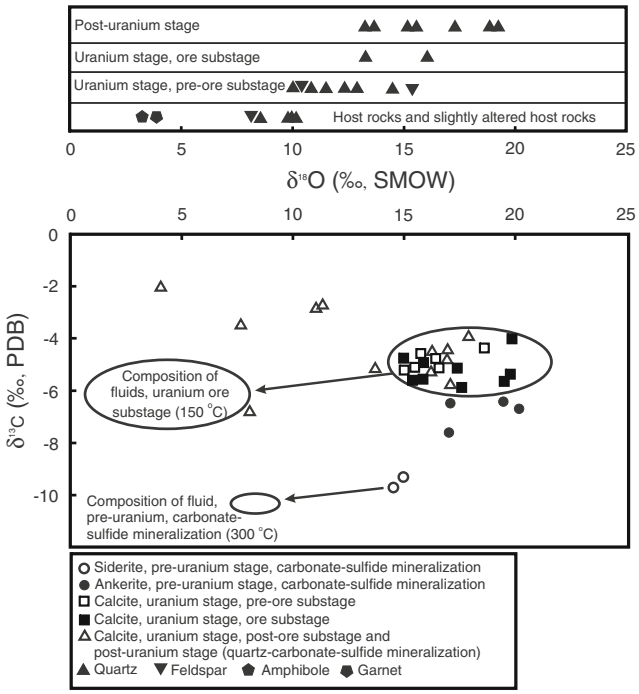


Fig. 15 Isotope composition of carbon and oxygen in individual types of hydrothermal carbonates, and isotope composition of quartz, feldspar, amphibole and garnet from the Rožná deposit. Ranges of isotope composition of carbon and oxygen in fluid are calculated for siderite and calcite K4

Oxygen and hydrogen

Oxygen isotope compositions of quartz, amphibole, and garnet from fresh or slightly retrograde-metamorphosed magmatic and metamorphic rocks (biotite and amphibole-biotite gneiss, anatectic granite) range between +3‰ and +11‰ SMOW and correspond to usual $\delta^{18}O$ values for metamorphic and magmatic rocks (Fig. 15). Feldspar and quartz analyzed from the uranium pre-ore and ore substages show a more positive range of $\delta^{18}O$ values (+9‰ to +l6‰ SMOW), and quartz of the post-uranium quartz-carbonate-sulfide mineralization has even higher values (+13‰ to +18‰ SMOW). The δD values determined for metamorphic biotite (−75‰ SMOW) and for white mica from the alteration that accompanies the pre-uranium carbonate-sulfide mineralization (−83‰ SMOW) plot in the δD range typical of metamorphic and magmatic rocks (Table 4).

During the pre-ore substage of the uranium mineralization, however, the δD values substantially increase (−39‰

Table 4 Isotope composition of oxygen and hydrogen of silicates in the host rock and altered host rock at the Rožná deposit

Sample/description	Mineral	$\delta^{18}O$ (‰ SMOW)	δD (‰ SMOW)
Metamorphic rocks			
HOR7/amphibole-biotite gneiss	Amphibole	+3.5	
	Biotite	+7.1	−75
HOR6/metagranite (garnet-biotite granitic gneiss)	K-feldspar	+8.2	
	Biotite	+7.1	−78
	Garnet	+3.3	
HOR4/biotite gneiss	Biotite	+10.2	−73
Retrograde-metamorphic alteration			
HOR5/retrograde-metamorphic quartz-muscovite vein	Muscovite	+7.8	−64
Pre-uranium stage alteration			
SP-8/hanging wall of sulfide-siderite vein	Sericite		−83
Uranium stage alteration, pre-ore substage			
ME-10/albitized and hematitized gneiss	Albite	+12.8	
	Chloritized biotite	+6.9	−41
ME-8/albitized and hematitized pegmatite	Albite	+16	
	Chloritized biotite	+7.4	−39
ME-1/albitized, chloritized and carbonatized biotite gneiss	K-feldspar	+14	
	Inherited chlorite[a]	+8.4	−47
ZA-14A/albitized and chloritized biotite gneiss	Authigennic chlorite	+8.8	−58
ZA-2/albitized, hematitized and carbonatized gneiss	Albite	+11	
	Authigennic chlorite	+7.3	−57
ZA-10/Chloritized and carbonatized gneiss	K-feldspar	+11.9	
	Authigennic chlorite	+8.0	−55
Uranium stage alteration, ore substage			
ZA-14A/Altered gneiss, hangingwall of uraninite-calcite vein	Albite	+12.6	
	Inherited, Fe-rich chlorite[a]	+11.2	−87
ZA-14B/Altered gneiss, footwall of uraninite-calcite vein	Inherited Fe-rich chlorite[a]	+10.9	−89

[a] Pseudomorph after biotite.

to −58‰; n=6). Because of difficulties with the separation of pre-ore and ore substage chlorites, only two samples of ore substage chlorite that overgrows uraninite accumulations were analyzed. The δD data of these chlorite samples are −87‰ and −89‰.

Temperature estimates obtained by sulfide thermometry, chlorite thermometry, and fluid inclusion studies were used for the calculation of the $\delta^{18}O$ and δD values of the fluid phases in equilibrium with the silicates and quartz analyzed (Fig. 16). The metamorphic fluids at Rožná range between +9.5‰ to +16.8‰ $\delta^{18}O$ and −45‰ to −58‰ δD, respectively, and correspond to the field of magmatic and metamorphic waters of Variscan Europe (Sheppard 1986). The δD value of fluids of the pre-uranium carbonate-sulfide mineralization, calculated using the δD value of white mica from the alteration halo (−40‰), plot in the same range, thus indicating a metamorphic origin. Fluids of the pre-ore substage of the uranium mineralization differ from the metamorphic fluids in their slightly lower $\delta^{18}O$ and substantially higher δD values (+6‰ to +10‰ and −30‰ to 0‰, respectively). The ore substage fluids differ from those of the pre-ore substage in their lower $\delta^{18}O$ and δD values (+2‰ to +7‰ and −37‰ to −39‰, respectively).

Timing of hydrothermal events

K–Ar age of illite, mica, and K-feldspar

Thirteen separates of biotite, muscovite, sericite-illite, and K-feldspar were used for K–Ar age determination. The K–Ar data on muscovite in retrograde-metamorphosed rocks and in sericite from wall rock of pre-uranium siderite veins range from 304.2±5.8 to 307.6±6.0 Ma, the K–Ar data on authigenic K-feldspar (adularia) and K-rich plagioclase from the pre-ore substage yielded ages of 296.3±7.5 to 281.6±5.4 Ma (Table 5).

The K–Ar ages determined for different grain size fractions of illite from ore substage argillic alteration range from 277.2±5.5 to 264.1±4.3 Ma depending on the grain size category and roughly correspond to the results of U–Pb dating of uraninite (280–260 Ma; Anderson et al. 1988). The K–Ar ages from post-uranium stage illite yielded ages of 233.7±4.7 to 227.5±4.6 Ma (Fig. 17).

Chemistry and chemical U–Pb age of monazite

Monazite grains from the host biotite gneiss yielded ages of 480±57 to 324±39 Ma (n=9; Table 6) and reflect variable

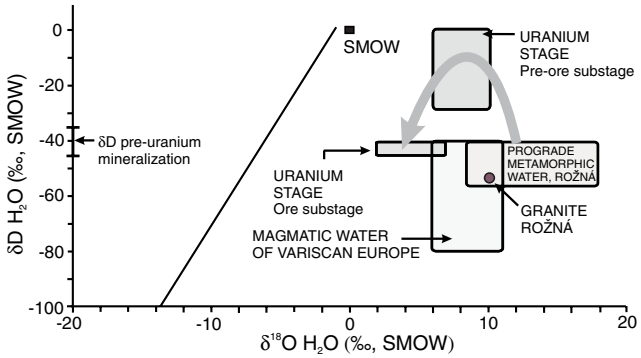


Fig. 16 Fields of oxygen and hydrogen isotope composition of solutions calculated for the individual mineralization stages and substages. The following fractionation equations were used: hydrogen in biotite–water and muscovite–water (Suzoki and Epstein 1976), chlorite–water (Savin and Lee 1988); oxygen in biotite–water and muscovite–water (Zheng 1993), chlorite–water (Cole and Ripley 1998). The following temperatures were used from mineral data: biotite of unaltered rocks 650°C, muscovite/sericite 300–350°C, pre-ore types of chlorite 300°C, ore stage chlorite 150°C. Data on $\delta^{18}O$ of hydrothermal quartz and calcite were also used to test the calculated $\delta^{18}O$ values of the solutions. The δD value of fluid of the pre-uranium ore stage mineralization was calculated using analysis of muscovite in the alteration zone of a carbonate-sulfide vein. The field of magmatic waters of Variscan Europe is after Sheppard (1986)

degree of Variscan metamorphic overprint in the Moldanubian domain (350–320 Ma; Schulmann et al. 2005) on the Cambrian to Mid-Devonian rock sequence. In addition to the igneous/metamorphic monazite, hydrothermally altered gneisses contain grains of newly formed, hydrothermal monazite in xenomorphic grains <10 μm across within fine-grained aggregates of authigenic chlorite and albite. Compared with monazite from nonaltered rocks that contain 0.44–0.70 wt% UO_2 and 2.13–5.13 wt% ThO_2, hydrothermal monazite is low in uranium (0.11–0.28 wt% UO_2) and variably depleted in thorium (0.1–4.3 wt% ThO_2). The chemical ages of the hydrothermal monazite are around 268±50 Ma (n=4, Table 6) and correspond to the ages obtained by U–Pb dating of uraninite (280 to 260 Ma; Anderson et al. 1988).

Graphite and organic geochemistry of bitumen

The host biotite gneiss at Rožná contains up to 0.4 wt% graphite (C_{graph}) in the form of lamellae up to 0.2 mm large. Reflectivity of graphite (R_{max}=10% to 13%, R_{min}=1.5% to 2.0%) and distinct optical anisotropy of graphite lamellae reveal a high structural ordering. The uraniferous mylonites and cataclasites of the Rožná shear zone have elevated C_{graph} contents (1.0 to 3.5 wt%). Graphite lamellae in slightly sheared rock are commonly bent and distorted. With an increase of plastic deformation, graphite flakes are pulverized to form black, submicroscopic particles that are concentrated, together with sericite and chlorite, in planes of maximum strain. There is no evidence of recrystallization or neoformation of graphite. During the superimposed brittle deformation, graphite pigment and fine-grained phyllosilicate particles were mechanically reconcentrated into "graphite seams" up to several millimeters thick.

Table 5 K–Ar ages of muscovite, K-feldspar, and illite from the Rožná deposit

Sample	Location	Description	Grain size (μm)	K (wt%)	^{40}Ar air (%)	$^{40}Ar_{rad}$ (nl/g)	Age (Ma)
HOR-5	PŠ4-212	Coarse-grained retrograde muscovite, quartz-muscovite veinlet	<5	4.3	5.59	54.86	307.6±8.7
SP-8	V_1-XVIII$_1$ VP RGS-R6 (20. vein)	Fine-grained white mica, alteration halo of the pre-uranium carbonate (siderite)-sulfide vein	<5	6.1	9.1	77.36	307.5±6.0
			<1	4.2	5.54	53.68	312.1±7.7
HOR-6	PŠ4-212	Coarse-grained K-feldspar, pre-ore substage of the uranium mineralization		4.7	4	61.56	312.0±6.2
ME-10	19A-1908	Coarse-grained K-feldspar, pre-ore substage, albitized and hematitized gneiss		5.6	4.2	58.98	308.0±7
ME-1	19A-1808	Authigenic adularia, pre-ore substage		6.9	4.1	79.94	281.6±5.4
ZA-10	1Z-16151	Authigenic, fine-grained adularia, pre-ore substage		3.4	10.3	41.14	296.3±7.5
ZA-21	1-2063	Illite, argillitized breccia with uranium mineralization (U mineralization slightly younger)	<5	4.4	9.3	50.62	277.2±5.5
			<3	5.3	8.3	60.9	276.1±5.1
			<1	6.6	4.8	74.85	274.9±4.7
ZA-13	1Z-15141	Illite, argillitized breccia with uranium mineralization (U mineralization slightly older)	<5	4.5	11.5	51.21	275.6±5.9
			<3	5.2	7.5	58.5	273.9±5.2
			<1	6.5	4.4	70.17	264.1±4.3
ZA-38	48-20117	Illite, argillitized hangingwall of the post-uranium, quartz-carbonate-sulfide mineralization	<5	3.6	4.4	34.54	233.7±4.7
			<3	3.6	4.5	34.22	231.5±4.5
			<1	3.7	4.7	34.03	227.5±4.6

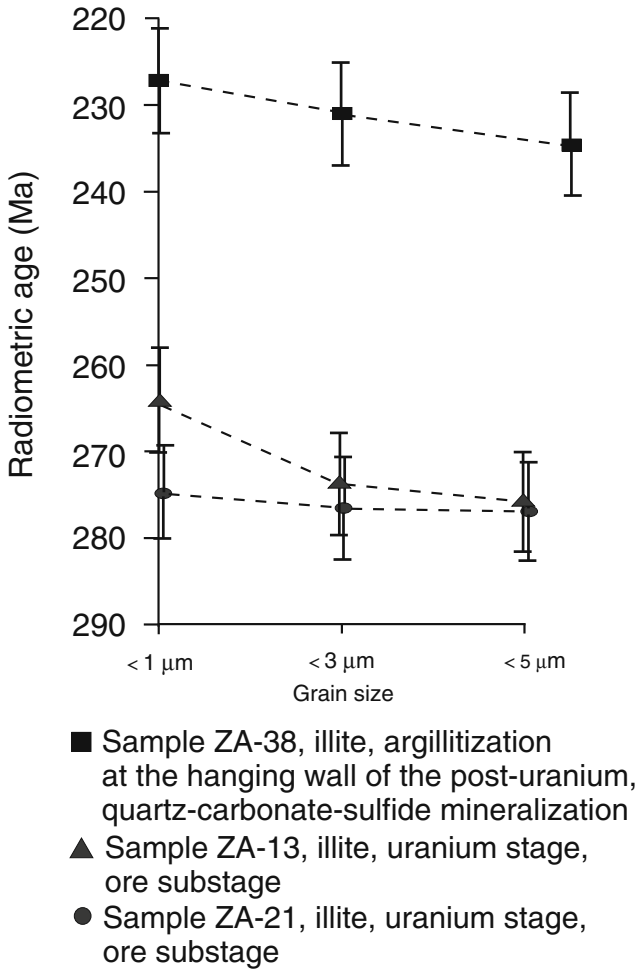


Fig. 17 K–Ar ages of grain size categories of illite from the ore stage of uranium mineralization, and of illite in altered rocks around post-uranium quartz-carbonate-sulfide mineralization

Besides the well-ordered graphite, rare solid bitumens were reported in uraniferous cataclasites at Rožná. These bitumens form globular or ribbon-like aggregates up to 1,000 μm across with numerous fragments of uraninite, coffinite, and (Zr,U)-silicate, which evidence the solidification of an originally liquid organic phase after the deposition of the main part of uranium ore (Fig. 7e). In contrast to graphite flakes, the bitumen aggregates do not display optical anisotropy. Rock samples with solid bitumens were chloroform-extracted. The extractable fraction yield was very low (<40 μg/100 g of rock). A typical reconstructed ion current spectrum of the extractable fraction (Fig. 18a) is characteristic of alkylderivative of benzene, indane, naphthalene, and aliphatic hydrocarbons, including isoprenoid biomarkers phytane and pristane, and shows a prominent chromatographic envelope in the n-C_{17} to n-C_{22} region, indicative of an irresoluble mixture of aliphatic and naphtenic compounds. The chromatographic pattern of extractable bitumens and the occurrence of biomarkers corroborate the idea that the origin of bitumens can be seen in hydrothermally altered oil products. The spectra of extractable organic matter from cataclasites at Rožná are similar to those obtained from uraniferous solid bitumens ("anthraxolite") from Permian sedimentary rocks of the Bohemian Massif (Fig. 18b) that originated due to diagenesis of the organic matter of Permian black shales (Fig. 18c).

Discussion

Mineral parageneses, sources of metals, and P–T–X characteristics of fluids

Pre-uranium stage The formation of the pre-uranium stage quartz-sulfide and carbonate-sulfide mineralizations at Rožná and the widespread pyritization, chloritization, sericitization, and carbonatization of the adjacent host rock can be related to a generally reduced retrograde-metamorphic fluid phase. The $\delta^{18}O$ of quartz and $\delta^{18}O$ and δD of mica in the alteration halos of both mineralization types are consistent with this interpretation. Variable liquid to vapor ratios and T_h CO_2 for inclusions in quartz of the quartz-sulfide and carbonate-sulfide mineralization and in quartz from retrograde-metamorphic quartz-muscovite veins indicate the trapping of inclusions under conditions of immiscibility of H_2O and CO_2 phases (below the solvus of the low-salinity H_2O–CO_2 system), at temperatures probably below 300°C. Using a different set of ore samples, Vosteen and Weinoldt (1997) and Hein et al. (2002) reported a similar temperature range (280°C to 300°C) for pre-uranium stage carbonate-sulfide mineralization. The results of the fluid inclusion studies correspond with the temperature estimate based on sulfide thermometry (approximately 300°C). Quartz-sulfide and carbonate-sulfide mineralizations, however, differ substantially in the isotope compositions of their sulfides. A wide range of $\delta^{34}S$ values of sulfides from the older quartz-sulfide mineralization ($\delta^{34}S$=+7‰ to +25‰) is attributed to local remobilization of sulfur from host rocks that contain sulfides and sulfates with mostly positive $\delta^{34}S$ values (Kříbek et al. 1996, 2002). In contrast, the narrow spread of the $\delta^{34}S$ data (−3‰ to +4‰) of the younger carbonate-sulfide mineralization points to a deep-seated, homogeneous sulfur reservoir and to focussed fluid flow along structural channels, i.e., ductile to brittle shear zones, during fracture propagation to the deeper crust. This scenario seems to be supported by the high $\delta^{18}O$ and low $\delta^{13}C$ values of carbonate (siderite and ankerite) indicative of a high-temperature equilibration of fluids with host rock, including hydrolytic decomposition of graphite.

Table 6 Concentrations of U, Th, and Pb, and chemical U–Pb age of monazite in the host rock and altered host rock at the Rožná deposit (concentrations in wt%)

Sample	Location	Description	UO_2	U	ThO_2	Th	Th*	Pb	Age (Ma)
Rožná-2	PŠ4-212	Monazite in quartz, biotite gneiss	0.44	0.392	3.24	2.852	4.139	0.086	468±56
Rožná-3a	1-1935	Monazite in feldspar, biotite gneiss	0.58	0.512	2.34	2.059	3.735	0.072	434±52
Rožná-3b	1-1935	Monazite in feldspar, biotite gneiss	0.55	0.483	2.13	1.875	3.464	0.073	480±57
Rožná-4a	1-1935	Monazite in feldspar, biotite gneiss	0.61	0.539	3.41	2.300	4.762	0.086	410±49
Rožná-4b	1-1935	Monazite in feldspar, biotite gneiss	0.52	0.461	2.67	2.348	3.844	0.055	324±39
Rožná-5a	4P-20111	Monazite in feldspar, biotite gneiss	0.70	0.619	3.96	3.476	5.497	0.095	390±47
Rožná-5b	4P-20111	Monazite in feldspar, biotite gneiss	0.54	0.475	5.13	4.509	6.055	0.091	336±40
Rožná-6	48-20117	Monazite in biotite, biotite gneiss	0.53	0.471	3.57	3.141	4.687	0.093	449±54
Rožná-7	48-20117	Monazite in feldspar, biotite gneiss	0.53	0.467	5.99	5.260	6.782	0.110	350±42
Rožná M-5-3	19A-1808	Hydrothermal monazite, pre-ore substage alteration, gneiss	0.11	0.099	0.11	2.415	2.736	0.035	286±66
Rožná M-5-1	19A-1808	Hydrothermal monazite, ore substage alteration, gneiss	0.28	0.250	3.33	2.928	3.736	0.044	264±48
Rožná M-5-2	19A-1808	Hydrothermal monazite, ore substage alteration, gneiss	0.18	0.159	3.02	2.656	3.172	0.037	260±57
Rožná-1	PŠ4-212	Hydrothermal monazite, ore substage alteration, gneiss	0.46	0.410	4.30	3.782	5.107	0.059	263±31

Th*is the apparent Th content calculated as a sum of measured Th and equivalent Th (equivalent of measured U content) using the software of Ludwig (1980). Analytical conditions: accelerating voltage=15 kV, probe current=250 mA. Counting times: Pb=240 s, background=2×120 s, Th=15 s, U=25 s. Errors: 0.04 wt% for Th, 0.025–0.030 wt% for U, and 0.010 wt% for Pb

Uranium stage As evidenced by prominent hematitization, especially in deeper parts of Rožná, the barren, pre-ore substage of the uraniferous fluid flow event indicates deep infiltration of oxidized, surface-derived fluids to the crystalline basement. Deep circulation of fluids of the pre-uranium substage gave rise to desilicified, hematitized, and albitized rocks. The petrological and geochemical character of the pre-ore altered rocks is very similar to that of episyenites described from numerous uranium deposits of the Variscan belt of Europe (Leroy 1984; Cathelineau 1986; Cuney et al. 1989). In contrast to episyenites, which are usually products of late magmatic alteration of granites, the hydrothermally altered rocks at Rožná are of metamorphic origin. The fluids responsible for the alteration of rocks of the pre-ore substage differ from the earlier low-salinity metamorphic fluids in their generally higher but highly variable salinities (7.3 to 21.8 wt% NaCl eq). Important differences in the salinity of the pre-uranium fluids probably reflect the large-scale mixing of chemically heterogeneous basinal brines with meteoric water. Compared with metamorphic fluids that produced the pre-uranium stage mineralization (mostly NaCl fluids), pre-ore substage fluids contain high amounts of $CaCl_2$ and possibly $MgCl_2$ and $FeCl_2$, which corresponds to the widespread albitization and hematitization of the host rock and formation of authigenic Mg-chlorites. The oxidized character of the fluids is evidenced by hematitization and the higher Fe^{3+}/Fe^{2+} ratio in chloritized biotite and protochlorite in hematitized rocks compared with the same ratio in chloritized biotite from pre-uranium alteration. Based on the Th of the aqueous inclusions, the temperature of the hydrothermal fluids of this substage can be estimated at 200°C. Hein et al. (2002) reported similar temperatures (T_h=179°C to 236°C) and lower salinities (1.1 to 8.1 wt% NaCl eq), based on fluid inclusion data on pre-ore substage carbonates. Chlorite thermometry of pre-ore, Mg-rich authigenic chlorites yielded temperatures in the range of 260°C to 310°C. These roughly correspond to the temperature calculated using the oxygen thermometer in the quartz–albite pair (Žák et al. 2001). Using the volumetric properties of fluid inclusions and pressure correction (Potter 1979), based on chlorite and isotope thermometers, the pre-ore mineralization (K1 and K2 calcite generation) is estimated to have formed at 0.6 to 1.3 kbar.

The isotope composition of the fluids of the pre-ore substage can be estimated at +6‰ to +10‰ $\delta^{18}O$ and 0‰ to −30‰ δD, respectively. The high $\delta^{18}O$ and δD values of pre-ore fluids can be best explained as due to the infiltration of basinal fluids from now eroded Late Stephanian and Early Permian cover rocks into the crystalline basement. Subtropical to tropical and, at least in some periods, arid climatic conditions are evidenced by the occurrence of anhydrite in Permian sedimentary rocks of the Bohemian Massif (Skoček et al. 1977). Elevated evaporation probably produced lake waters with relatively high $\delta^{18}O$ and δD characteristics. For the Permo-Triassic waters of Europe, Wilkinson et al. (1995) reported δD values between −14‰ and −3‰. Turpin et al. (1981) calculated δD of −5‰ for

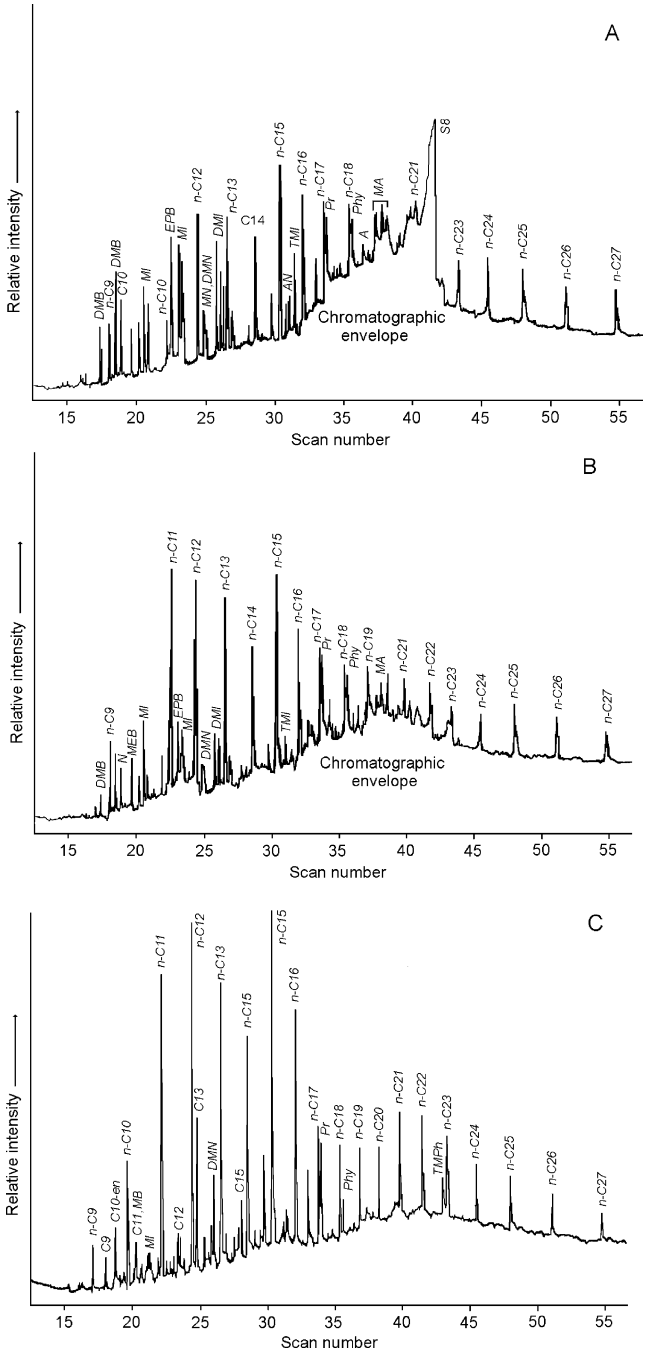


Fig. 18 Reconstructed chromatogram (total ion current) of a chloroform extract from ore-bearing cataclasites of the Rožná deposit (**a**), from uranium-bearing bitumen ("anthraxolite") of the Permian sedimentary rocks (**b**), and from Permian black shale of the Bohemian Massif (**c**). *AN*: alkylnaphthalenes, *n-Cx*: *n*-alkanes, *Cx*: isoalkanes, *Cx-en*: alkenes, *DMB*: dimethylbenzenes, *DMI*: dimethylindanes, *DMN*: dimethylnaphthalenes, *EPB*: ethylpropylbenzene, *MA*: methylanthracene, *MEB*: methylethylbenzenes, *MA*: methylanthracenes, *MI*: methylindanes, *MN*: methylnaphthalenes, *N*: naphthalene, *Pr*: pristane, *Phy*: phytane, *S8*: octahedral sulfur, *TMA*: trimethylanthracenes, *TMI*: trimethylindanes, *TMPh*: trimethylphenanthrenes

basinal fluids giving rise to the late Variscan vein mineralization of Portugal. The $\delta^{18}O$ and δD characteristics of basinal brines can be shifted to even higher values on fluid–evaporite interaction (Sheppard 1986). The reaction of basinal waters with hematite and anhydrite will lead to an oxidation state of the fluid well above the magnetite-hematite buffer (Sverjensky 1987). Oxidizing basinal brines can be very effective in leaching uranium. Compared with the average contents of uranium and thorium in Moldanubian gneisses (3.6 ppm U, 11.1 ppm Th, Th/U=3.22, n=68; René 2002), unaltered host gneiss and migmatites of the Rožná-Olší uranium ore field are generally slightly enriched in uranium (5.2 ppm U, 8.4 ppm Th, Th/U= 3.27, n=14). Uranium in host gneisses and migmatites is essentially hosted by monazite, which contains 5.4 wt% Th and 0.9 wt% U on average, and to a lesser extent, by thorogummite, cheralite, and zircon (Leichmann et al. 2002). In barren, pre-ore substage hydrothermally altered rocks, monazite, thorogummite, and cheralite are missing and zircon is slightly corroded. Therefore, the source of uranium may be in the hydrothermal decomposition of uranium-bearing accessories, as proposed for the unconformity-type uranium deposits in Canada by Hecht and Cuney (2000). A similar scenario, i.e., the extraction of uranium from crystalline rocks by Permian formation waters was proposed by Turpin et al. (1990) to explain the origin of uranium in hydrothermal uranium deposits in Hercynian granites of the Massif Central, France.

Uranium mineralization followed, or partly overlapped in time, the pre-ore substage alteration. Uranium-enriched fluids were probably driven in the direction of thermal and pressure gradients toward the permeable zones of pyritized and graphite-enriched cataclastic zones that frequently cut and displace pre-ore altered rocks. Several generations of ore and gangue fault breccia cemented by carbonate and, to a lesser extent, by quartz document multiple opening and healing of the ore-controlling brittle structures and the possibility of tectonically driven flow and seismic pumping of ore-bearing fluids. In the same time period, the porous, albitized, and hematitized rocks that originated during the pre-ore alteration substage served as a "trap" for the uranium mineralization. The same scenario was proposed for uranium-bearing episyenites at uranium deposits of the Massif Central in France (Leroy 1984). Uranium mineralization is represented by uraninite and at least two generations of Y-rich coffinite (commonly zirconium-enriched coffinite); brannerite being far less abundant. In addition to zirconium-enriched coffinite, (U,Zr)-silicate phase was detected in the ore. U-silicate phase with 64 at. % Zr was recorded in bitumens at the Oklo-Okélobondo uranium deposit in Gabon by Jensen and Ewing (2001). At Rožná, uranium is bound by microheterogeneous substances formed by a mixture of U, Ti, Si, Ca, Fe, and Zr. High

concentrations of these generally immobile elements, i.e., Ti, Y, and Zr, in hydrothermal fluids are usually attributed to the formation of fluoride or phosphate complexes (Gieré 1990; Rasmussen 2005). However, apatite and monazite occur only as accessories in hydrothermally altered rocks associated with uranium mineralization, and fluorite forms a part of the younger post-uranium quartz-carbonate-sulfide mineralization. In F- and P-poor hydrothermal systems, the mobility of Ti, Y, and Zr may be promoted by sulfate complexing (Rubin et al. 1993). Oxidation of pyrite and formation of anhydrite during the emplacement of the uranium mineralization at Rožná are consistent with this scenario. Selenide mineralization that accompanies uraninite and coffinite is slightly younger than uranium mineralization. As relatively high concentrations of selenium were reported from pre-uranium sulfides by Vencelides (1991), it is highly probable that the oxidation of rock sulfides during the introduction of oxidative, uranium-bearing fluids resulted in the oxidation of both sulfur and selenium. Contrary to SO_4^{2-}, SeO_4^{2-} can be easily reduced to form selenides at relatively high oxidation state. This scenario is consistent with the occurrence of both anhydrite and selenides in ore substage hydrothermally altered host rocks. P–T–X conditions of the ore substage of the uranium mineralization can be estimated using fluid inclusion, stable isotope, and chlorite thermometry data. The T_h values of primary inclusions range between 152°C and 174°C, and their total salinities span a relatively wide interval of 3.1 to 23.1 wt% NaCl eq. Hein et al. (2002) obtained a similar temperature (T_h=130–166°C) for primary inclusions of the ore stage K3 and K4 carbonates, but lower salinity (3.1 and 7.7 wt% NaCl eq). Isotope compositions of oxygen and hydrogen in Fe-rich ore substage chlorite differ from those of pre-ore chlorite. Percival et al. (1993) reported a similar difference between pre-ore and Fe-rich ore chlorites for the Cigar Lake uranium deposit in Saskatchewan, Canada. Using the data of Suzoki and Epstein (1976), they interpreted the differences in the δD isotope composition as a result of a higher concentration of D in Mg- and Al-rich hydrous minerals relative to Fe-bearing minerals. However, taking into account the significant differences between the δD values of pre-ore and ore chlorites at Rožná, it cannot be ruled out that the δD values for ore chlorite reflect an oxidation of the D-depleted organic molecules in the hydrothermal solution (organic waters, Sheppard 1986).

Uranium precipitation can be controlled by many factors, including a decrease in temperature and pressure, mixing, boiling, and degassing of fluids, decrease in pH, or a decrease in oxygen fugacity (Evert et al. 1997). Moreover, sorption and subsequent reduction of uranium species on the surface of silicates or hydrooxides of iron may play a substantial role in uranium immobilization. Fluid inclusion studies at Rožná provided no evidence of boiling or degassing of uraniferous fluids. Multiple dissolution and reprecipitation of several generations of carbonates as evidenced by CL studies indicate that the pH of the uranium-bearing solutions varied slightly along the boundary of the carbonate stability field. As kaolinite is entirely missing in the hydrothermally altered rocks, the pH of the solutions was probably buffered by the equilibrium between illite and K-feldspar in the range of 7 to 8. Typical alterations that accompany uranium mineralization include the formation of Fe^{3+}-enriched chlorite and the decomposition of previously formed chloritized biotite, protochlorite, and matrix chlorite to Fe-rich illite and hydrooxides of iron (goethite and amorphous Fe hydrooxides). The large extent of altered rocks and the abundant presence of Fe^{3+}-bearing minerals associated with the uranium ore suggest that the deposition of uranium minerals was a response to the reduction of the ore-bearing fluid by direct interaction with ferrous iron-bearing silicate (biotite and chlorite). A similar scenario was proposed for Australian deposits by Wilde et al. (1989). In addition to Fe^{2+} phyllosilicates, pre-uranium pyritization significantly contributed to the reducing capacity of the host rock. In contrast, the role of graphite in the ore-bearing solution is probably negligible due to the low reactivity of graphite at temperatures below 300°C (French 1966; Frost 1979).

Homogenization temperatures of post-ore substage carbonate inclusions range between 84°C and 131°C. Compared with the ore substage inclusions, the salinities are lower (0.5 and 12.4 wt% NaCl eq), which may indicate increasing mixing of formation water with surface-derived rainwater. Hein et al. (2002) reported almost the same homogenization temperatures (80°C to 130°C) for inclusions from post-ore substage carbonates but higher salinities (10.5 to 18.6 wt% NaCl eq). The pressures of 0.2 and 0.7 kbar were estimated for the post-ore mineralization (K5–K6 calcite generation) after pressure correction (Potter 1979) using chlorite and stable isotope thermometers. Exceptional low-density CH_4 inclusions of this substage can represent either secondary overprinted, reequilibrated older inclusions or products of radiation-induced polymerization of organic molecules as was proposed for the Příbram uranium deposit by Kříbek et al. (1999) and for Canadian uranium deposits by Landais and Dereppe (1985) and Wilson et al. (2003). Because of the occurrence of solid uraniferous bitumens at Rožná, we prefer the second possibility. The origin of organic molecules during diagenetic and catagenetic transformation of organic matter of the Stephanian and Lower Permian sedimentary rocks was documented by the presence of biogenic tracers (phytane and pristane, i.e., products of the diagenetic decomposition of the chlorophyll molecule) in extractable parts of bitumens at Rožná.

Post-uranium stage The chalcocite-pyrrhotite-pyrite-chalcopyrite-galena mineral assemblage of the post-uranium stage and the disequilibrium assemblage of pyrrhotite and barite indicate variable sulfidation state. This variation is also expressed in the distinct zoning of carbonate and quartz crystals as revealed by CL images (Kříbek and Hájek 2005; Vosteen and Weinoldt 1997). Fluid inclusions in quartz that forms part of the early mineral paragenesis have T_h of 165°C to 178°C and very high salinities around 25 wt% NaCl eq (Hein et al. 2002 report 14.0 to 18.6 wt% NaCl eq). Temperatures obtained for the early stage of mineralization range from 100°C to 200°C using the galena-sphalerite sulfur isotope thermometer and from 170°C to 190°C using the chlorite thermometer. The pressure of trapping of quartz-calcite-sulfide mineralization (K7 calcite generation in association with early quartz and sphalerite) was estimated at 0.2 to 0.4 kbar. Low-salinity inclusions in paragenetically younger K7 carbonates, barite, and associated quartz (3.2–16.3 wt% NaCl eq) probably document an increasing mixing of residual brines in crystalline rocks ("shield brines"; Negrel and Casanova 2005; Leybourne et al. 2006) derived from external sources (brines of Permian basins) or generated in situ by low-temperature crystalline rock–water interactions with meteoric water. In drusy quartz, monophase liquid-only inclusions are present indicating low temperatures (<100°C) of the latest stage of mineralization. The wide spread of sulfide sulfur isotope data indicates either a remobilization of sulfur from older stratabound mineralization that occurs in the host rocks at Rožná or, more likely, a different degree of isotope fractionation between oxidized (sulfate) and reduced (sulfide) forms of sulfur species in the fluid.

Timing of the mineralization and relation to the late Variscan and post-Variscan geological evolution of the Bohemian Massif

The various types of hydrothermal mineralization at Rožná can be correlated with (1) post-orogenic extension of the Variscan crust accompanied by a rapid exhumation and tectonic ablation of crustal blocks during the Late Westphalian, (2) late Variscan transcurrent tectonics and opening of Stephanian and Lower Permian basins, and with (3) early stage of rifting in the Thetys-Central Atlantic region in the Middle and Late Triassic (Fig. 19).

(Ad 1) All mineralization styles at Rožná are bound to faults and conjugate structures of the shear zone that originated in the upper part of the passively transported Moldanubian nappes during the deep-level core wedging of the Brunovistulian in the east beneath the Moldanubian orogenic root between 340 and 337 Ma (Schulmann et al. 2005). The structures were reactivated during NE–SW dextral transpressive shearing parallel to the Brunovistulian foreland at 330–325 Ma (Schulmann et al. 2005) and later, during the early stage of post-orogenic extension in the Moldanubian domain (325 to 300 Ma; Handler et al. 1991). The K–Ar radiometric ages of white mica from the Rožná mylonites (307.6±8.7 Ma) and from sericite in the wall rock of the siderite-sulfide veins (312±6.0 to 307±7.7 Ma) are consistent with the time span of the post-orogenic extension. It can be, therefore, hypothesized that the origin of fluids giving rise to the quartz-sulfide and carbonate-sulfide mineralizations at Rožná was related to the isothermal decompression, uplift, and hydration of the upper crust following overthrusting and large-scale melting of the lower crust of the Moldanubian domain. This model was suggested for many late Variscan siderite-sulfide vein-type deposits of Variscan Europe (Hein 1993; Radvanec et al. 2004).

(Ad 2) Uranium mineralization is significantly separated in time from the previous stage. Radiometric K–Ar dates of authigenic K-feldspar (adularia) in albitized and hematitized rock of the pre-ore substage (296.3±7.5 and 281±7.0 Ma) correspond to the opening of the Late Stephanian to Lower Autunian transpressional or transtensional grabens in the Bohemian Massif (Pešek et al. 2001). The regional distribution of the Late Stephanian and Permian sedimentation in the Bohemian Massif was probably much more extensive compared to the now preserved remnants. Franců et al. (1998), for example, using reflectance data of organic matter in Permian basins, documented that at least 2,800 m of Autunian and younger sediments were eroded in the Boskovice Graben (Fig. 2) before the Early Cretaceous. The initial stage of graben formation (300 to 290 Ma) was characterized by differential block movement in a generally brittle deformation regime. The uranium-enriched basinal fluids were transported along the direction of pressure and temperature gradients, i.e., toward the cataclastic, chloritized and pyritized zones in the time span of 280 to 260 Ma (K–Ar illite and chemical U–Pb monazite dating). These ages correspond with previously published U–Pb ages on uraninite of 280 to 260 Ma (Anderson et al. 1988). The circulation of hydrothermal fluids probably ceased because of the tectonic inversion of the Lower Permian basins during the Late Autunian and Saxonian.

(Ad 3) Radiometric K–Ar ages of illite in the host rock of the post-uranium stage (quartz-carbonate-sulfide

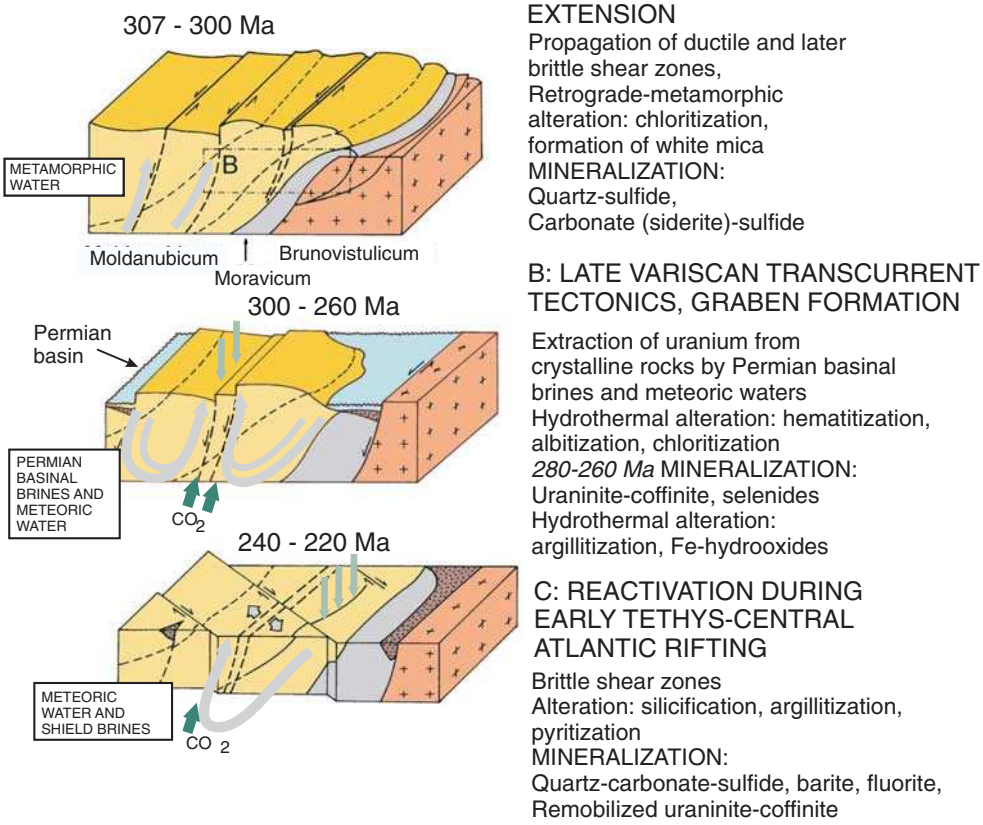


Fig. 19 Model of the fluid evolution at the Rožná uranium deposit in relation to the geodynamic evolution of the Bohemian Massif in late Variscan and early post-Variscan times

mineralization) of 233.7±4.7 to 227.5±4.6 Ma reveal a reactivation of uranium-bearing cataclastic shear zones during the Middle to Late Triassic. Tectonic and thermal reactivation of ore-bearing structures and the formation of new, crosscutting faults can be probably attributed to the post-Variscan, early Alpine transcurrent movements all over central Europe (Brandmayr et al. 1995). The reactivation of Variscan and pre-Variscan structures in this period probably reflects the early tensional phase in the Paleotethys-Central Atlantic region (Ziegler 1996).

Conclusions

Our data allow to establish a genetic model of the shear zone-hosted uranium deposit at Rozna and to integrate the mineralization history into the late Variscan and post-Variscan geological evolution of the Bohemian Massif. The origin of the pre-uranium, quartz-sulfide, and carbonate-(siderite-ankerite)-sulfide mineralizations is related to post-orogenic extension of the Moldanubian crust that was accompanied by retrograde-metamorphic alteration of high-grade mylonitized rocks and cataclasites during the West-phalian. Within this period, rocks of the shear zone were pyritized and chloritized, thus forming favorable redox traps.

The origin of the uranium mineralization is associated with infiltration of oxidized basinal brines of the Upper Stephanian and Lower Permian basins into the crystalline basement along deep brittle structures that opened during the late Variscan transcurrent crustal block reorganization. Relicts of Upper Carboniferous and Lower Permian clastic sedimentary rocks in the Moldanubian domain indicate that the areal extent of the Permian sedimentation was much larger than today. It is, therefore, highly probable that Permian sedimentary rocks unconformably covered a substantial part of the periphery of the Moldanubian domain. Infiltration of basinal brines effectively leached uranium from U-bearing accessories and silicates in the crystalline rocks. Quick uplift and tectonic ablation of the basement enabled seismic pumping of ore-bearing fluids toward the chloritized and pyritized zones of cataclasites where uranium was gradually precipitated due to the interaction of ore fluids with reducing host rock lithologies (ferrous silicates and pyrite). The principal role of formation waters of the Upper Stephanian and Permian basins in the origin of uranium mineralization at Rožná thus parallels the model for unconformity-type uranium deposits in Canada and Australia. Within this scenario, the Rožná

deposit may represent the basement rock-hosted part of an unconformity-type deposit, the overlying Permian sedimentary cover being almost entirely eroded during the pre-Cretaceous period. Compared with the spatially restricted but high-grade unconformity-type deposits, the relatively large extent of the uranium mineralization and the low ore grade at Rožná points to a relatively defocused fluid system.

In the Middle to Late Triassic, zones of uraniferous cataclasites were reactivated and crosscut by newly formed fault systems. During this hydrothermal event, uranium mineralization was locally remobilized and quartz-carbonate-sulfide mineralization formed. The wide range of salinities of fluids probably documents mixing of residual brines in crystalline rocks ("shield brines") with meteoric water.

In the context of hydrothermal uranium mineralization of the Variscan belts of western and central Europe, the Rožná uranium deposit and some other deposits of the Moldanubicum of the Bohemian Massif (such as the Mähring, Olší, Dyleň, Zadní Chodov, Okrouhlá Radouň deposits) differ from those of the Massif Central and Armorican Massif in France and from those in the Erzgebirge (Krušné hory Mountains) in Germany/Czech Republic. "Disseminated-type" uranium deposits of the Massif Central and Armorican Massif are generally linked with plutons of fractionated muscovite granites, which are considered the main source of uranium. Rožná and other deposits of the Moldanubicum of the Bohemian Massif show no spatial relationship between mineralization and granitic plutons. Apart from the generally vein-type deposits in the Erzgebirge (Krušné hory Mountains) and the Příbram uranium deposit, which are characterized by the proximity of granitic plutons and by very weak hydrothermal alteration, the Rožná deposit shows extensive albitization, chloritization, and hematitization of the crystalline country rocks and a mostly disseminated style of mineralization. Reactions of hydrothermal fluids with the host rocks can also be held responsible for the much wider variability in chemical composition of the fluids compared to the vein-type deposits. On the other hand, a feature common to all uranium deposits of Variscan Europe is their approximately same age (280–260 Ma) and their spatial association with tectonic structures formed or reactivated in the latest Stephanian or Early Permian. Hydrothermal fluid circulation along structures controlling the mineralization was probably accelerated by elevated heat flow. This is evidenced by the high coalification degree of the Stephanian coal (up to the anthracite stage) in the pull-apart basins which developed on these structures.

Acknowledgments This study is based on results of tens of unpublished, and formerly held secret, reports available exclusively from the archives of the Diamo State Enterprise. For many years, the deposit was studied by Russian geologists, i.e., I.M. Bayushkin, V. Ye. Boytsov, J.M. Dymkov, P.A. Ivanov, B.P. Yurgenson, V.S. Katargin and, at different stages of exploitation, by Czech geologists, i.e., F. Fediuk, J. Komínek, M. Kvaček, J. Malec, F. Novák, P. Pauliš, V. Rozhoň, Z. Uhlík, S. Vilhelm, J. Vokoun, V. Zrůstek, and many others. The present paper could have never originated without their detailed geological, mineralogical, and structural studies.

The manuscript benefited from reviews by M. Pagel and an anonymous reviewer. Last but not the least, we wish to thank P. Sulovský and J. Zimák for their interpretation of chlorite chemistry, I. Vavřín, Z. Korbelová, and V. Šrein for microprobe analyses, J. Schneeweis for Mössbauer spectra of phyllosilicates, B. Humer for the determination of chemical U–Pb ages of monazite, and J. Adamovič for his English corrections.

References

Anderson EB, Ivanov PA, Komínek J (1988) Ore metasomatism at the uranium veins of the Rožná deposit. Geol Hydrometal Uranium 12:70–88 (in Czech with English summary)

Arapov JA, Bojcov VJ, Česnokov NI, Djakonov AV, Halbrštát J, Jakovjenko AM, Kolek M, Komínek J, Kozyrev VN, Kremčukov GA, Lažanský M, Milovanov V, Nový C, Šorf F (1984) Uranium deposits of the Czechoslovakia. Czechoslovak Uranium Industry, Prague, p 420 (in Czech with English summary)

Bakker RJ, Diamond LW (2000) Determination of the composition and molar volume of H_2O-CO_2 fluid inclusions by microthermometry. Geochim Cosmochim Acta 64:1753–1764

Bodnar RJ, Vityk MO (1995) Interpretation of microthermometric data for H_2O–NaCl fluid inclusions. In: De Vivo B, Frezzotti ML (eds) Fluid inclusions in minerals: methods and applications. Short course of the working group "Inclusion in Minerals". Virginia Polytechnic Institute, Blacksburg, VA, pp 117–130

Borisenko AS (1977) Cryotechnic methods for the determination of fluid inclusions salts in minerals. Geol Geofiz 8:16–27 (in Russian)

Brandmayr M, Dallmeyer RD, Handler R (1995) Conjugate shear zones in the Southern Bohemian Massif (Austria)—implications for Variscan and Alpine tectonothermal activity. Tectonophysics 248:97–116

Cathelineau M (1986) The hydrothermal alkali metasomatism effects on granitic rocks: quartz dissolution and related subsolidus changes. J Petrol 27:945–965

Cathelineau M (1988) Cation site occupancy in chlorites and illites as a function of temperature. Clay Miner 23:471–485

Cathelineau M, Nieva D (1985) A chlorite solid solution geothermometer. The Los Azufres (Mexico) geothermal system. Contrib Mineral Petrol 91:235–244

Clayton RN, Mayeda TK (1963) The use of bromine pentafluoride in the extraction of oxygen from oxides and silicates. Geochim Cosmochim Acta 27:43–52

Cole DR, Ripley EM (1998) Oxygen isotope fractionation between chlorite and water from 170–350°C: A preliminary assessment based on partial exchange and fluid/rock experiments. Geochim Cosmochim Acta 63:449–457

Cuney M, Leroy J, Molina P (1989) Metalogenesis in the French part of the Variscan orogen. Part 1. U-preconcentration in the pre-Variscan and Variscan formations—a comparison with Sn, W and Au. Tectonophysics 117:39–57

Deer WA, Howie RA, Zussman J (1964) Rock-forming minerals. Volume 3. Sheet slilicates. Longman, London

Dobeš P, Žák K, Kříbek B (2001) Fluid inclusion and stable isotope study of the Rožná uranium deposit, Czech Republic. In: Noronha F, Dória A, Guedes A (eds) ECROFI XVI, European Current Research on Fluid Inclusions, Porto 2001, Abstracts, Universidade do Porto, pp 115–117

Evert L, Shock DC, Sassani C, Betz H (1997) Uranium in geologic fluids: Estimates of standard partial molar properties, oxidation potentials, and hydrolysis constants at high temperatures and pressures. Geochim Cosmochim Acta 61:4245–4266

Franců J, Sýkorová I, Franců E, Šafanda J, Malý L (1998) Vitrinite reflectance of coals in the Boskovice Furrow as related to thermal and burial history. In: Pešek J, Opluštil O (eds) VIII. Coal Geology Conference, Abstracts, Charles University, Prague, pp 28

Franke W (2006) The Variscan orogen in Central Europe: construction and collapse. In: Gee DG, Stephenson RA (eds) European lithosphere dynamics. Geological Society, London, Memoires 32, pp 334–343

French BM (1966) Some geological implications of equilibrium between graphite and a C-H-O gas phase at high temperatures and pressure. Rev Geophys 4:223–253

Frost BR (1979) Mineral equilibria involving mixed-volatiles in a C–O–H fluid phase: the stabilities of graphite and siderite. Am J Sci 279:1033–1059

Fuchs G (1986) Zur Diskussion um den Deckenbau der Boehmischen Masse. Jahrb Geol Bundesanst 129:41–49

Gieré R (1990) Hydrothermal mobility of Ti, Zr and REE: examples from the Bergell and Adamello contact aureoles (Italy). Terra Nova 2:60–67

Grinenko VA (1962) Preparation of sulfur dioxide for isotopic analyses. Zhurnal Neorganiceskoi Chimii 7:2479 (in Russian)

Handler R, Brandmayr M, Dallmeyer RD, Wallbrecher E (1991) Age and kinematics of shear zones in the southern Bohemian Massif. In: Anonymous (ed) Sixth Meeting of the European Union of Geosciences, Terra abstracts 3. Blackwell Scientific, Oxford, pp 206

Hecht L, Cuney M (2000) Hydrothermal alternation of monazite in the Precambrian crystalline basement of the Athabasca Basin (Saskatchewan, Canada): implications for the formation of unconformity-related uranium deposits. Miner Depos 35:791–795

Hein UF (1993) Synmetamorphic Variscan siderite mineralization of the Rhenish Massif, Central Europe. Mineral Mag 57:451–467

Hein UF, Lehmann B, Kříbek B, René M (2002) Evolution of ore-forming fluids along the Rožná-Olší shear zone, Bohemian massif, Czech Republic: implication for local uranium deposition and comparison with U-mineralization at Schlema, Erzgebirge, Germany. In: Kříbek B, Zeman J (eds) Uranium deposits: from their genesis to their environmental aspects. Proceedings of the International Workshop, Czech Geological Survey, Prague, pp 61–64

Hendel EM, Hollister LS (1981) An empirical solvus for CO_2–H_2O–2.6 wt. % salt. Geochim Cosmochim Acta 45:225–228

Hey MH (1954) A new review of the chlorites. Mineral Mag 30:277–292

Jensen KA, Ewing RC (2001) The Okélobondo natural fission reactor, southeast Gabon: Geology, mineralogy, and retardation of nuclear-reaction products. Geol Soc Amer Bull 113:32–62

Johan Z, Kvaček M (1971) La bukovite, $Cu_{3+x}Tl_2FeSe_{4-x}$, une nouvelle espéce minérale. Bull Soc Géol Mineral Crystallogr 94:529–533

Johan Z, Kvaček M, Picot P (1976) Petrovicite, $Cu_3HgPbBiSe_5$, a new mineral. Bull Soc Géol Mineral Crystallogr 99:310–313

Johan Z, Kvaček M, Picot P (1978) La sabatierite, un nouveau seléniure de cuivre et de thallium. Bull Soc Géol Mineral Crystallogr 99:310–313

Jowett EC (1991) Fitting iron and magnesium into hydrothermal chlorite geothermometer. GAC/MAC/SEG Joint Annual Meeting, Program with Abstracts, Toronto, A62, pp 16

Kapusta Y, Steinitz G, Allerman A, Sandler A, Kotlarsky P, Nagler A (1997) Monitoring the deficit of Ar-39 in irradiated clay fractions and glauconites: modelling and analytical procedure. Geochim Cosmochim Acta 61:4671–4678

Kotková J, Schaltegger U, Leichmann J (2003) 338–335 Ma old intrusion in the E Bohemian Massif—a relict of the orogen-wide durbachitic magmatism in European Variscides. J Czech Geol Soc 48:80–81

Kříbek B, Hájek A (eds) (2005) The Rožná uranium deposit. Czech Geological Survey, Prague, p 163 (in Czech with English summary)

Kříbek B, Hladíková J, Holeczy D (2002) Anhydrite-bearing rocks from the Rožná district (Moldanubian zone, Czech Republic: high-grade metamorphosed exhalites? Miner Depos 37:465–479

Kříbek B, Hladíková J, Žák K, Bendl M, Pudilová M, Uhlík Z (1996) The barite-hyalophane sulfidic ores at Rožná, Bohemian Massif, Czech Republic: metamorphosed black shale-hosted submarine exhalative mineralization. Econ Geol 91:14–35

Kříbek B, Žák K, Spangenberg J, Jehlička J, Prokeš S, Komínek J (1999) Bitumens in the Late Variscan hydrothermal vein-type uranium deposit of Příbram, Czech Republic: sources, radiation-induced alteration, and relation to mineralization. Econ Geol 94:1093–1114

Kröner A, O'Brien PJ, Nemchin AA, Pidgeon RT (2000) Zircon ages for high pressure granulites from South Bohemia, Czech Republic, and their connection to Carboniferous high temperature processes. Contrib Mineral Petrol 138:127–142

Landais P, Dereppe JM (1985) A chemical study of the carbonaceous material from the Carswell structure. In: Laine R, Alonso D, Šváb M (eds) The Carswell structure. Uranium deposits, Saskatchewan. Geol Assoc Can Spec Pap 29:165–174

Leichmann J, Matula M, Broska I, Holeczy D (2002) Low-degree partial melting of metapelites—another possible implement for selective concentration of uranium: example from the Rožná uranium deposit, Bohemian Massif. In: Kříbek B, Zeman J (eds) Uranium deposits: from their genesis to their environmental aspects. Proceedings of the International Workshop, Czech Geological Survey, Prague, pp 75–78

Leroy J (1984) The episyenitization in uranium deposit in Bernardan (Marche)—comparison with similar deposits of northwestern area of the French Massif Central. Miner Depos 19:26–35

Leybourne MI, Clark ID, Goodfellow WD (2006) Stable isotope geochemistry of ground and surface waters associated with undisturbed massive sulfide deposits; constraints on origin of waters and water-rock reactions. Chem Geol 231:300–325

Ludwig F (1980) Calculations of uncertainties of U–Pb isotope data. Earth Planet Sci Lett 46:212–220

Matté P, Maluski H, Rajlich P, Franke W (1990) Terrane boundaries in the Bohemian Massif: Result of large-scale Variscan shearing. Tectonophysics 177:151–170

Matura A (1984) Das Kristallin am Suedostrand der Boehmischen Masse zwischen Ybbs/Donau und St. Poelten. Jahrb Geol Bundesanst 127:13–27

McCrea JM (1950) The isotopic chemistry of carbonates and a paleotemperature scale. J Chem Phys 18:849–857

Montel JM, Foret S, Veschambre M, Nicollet Ch, Provost A (1996) A fast reliable inexpensive in-situ dating technique: Electron microprobe ages on monazite. Chem Geol 13:37–53

Negrel P, Casanova J (2005) comparison of the Sr isotopic signatures in brines of the Canadian and Fennoscandian shields. Appl Geochem 20:749–766

OECD-IAEA (2003) Uranium 2002. OECD Nuclear Energy Agency and International Atomic Energy Agency, Vienna, Paris, p 156

Ohmoto H, Rye RO (1979) Isotopes of sulfur and carbon. In: Barnes HL (ed) Geochemistry of hydrothermal ore deposits. 2nd edn. Wiley, New York, p 482

Percival JB, Bell K, Torrance JK (1993) Clay mineralogy and isotope geochemistry of the alteration halo at the Cigar Lake uranium deposit. Can J Earth Sci 30:689–704

Pešek J, Holub V, Jaroš J, Malý L, Martínek K, Prouza V, Spudil J, Tásler R (2001) Geology and mineral deposits of the Upper Palaeozoic limnic bassins of the Czech Republic. Czech Geological Survey, Prague, p 244 (in Czech with English summary)

Potter RW (1979) Pressure corrections for fluid-inclusion homogenization temperatures based on the volumetric properties of the NaCl–H_2O. J Res US Geol Surv 5:603–607

Poty B, Leroy J, Jachimowicz L (1976) Un nouvel appareil pour la mesure des temperatures sous le microscope: L'installation de microthermometrie Chaixmeca. Bull Soc Géol Mineral Crystallogr 99:182–186

Radvanec M, Grecula P, Žák K (2004) Siderite mineralization of the Gemericum superunit (Western Carpathians, Slovakia): review and a revised genetic model. Ore Geol Rev 24:267–298

Rasmussen B (2005) Zircon growth in very low grade metasedimentary rocks: evidence for zirconium mobility at ~250°C. Contrib Mineral Petrol 150:146–155

René M (2002) The REE–U–Th distribution in hydrothermally altered rocks at the Rožná uranium deposit, Czech Republic. In: Kříbek B, Zeman J (eds.) Uranium deposits: From their genesis to their environmental aspects. Proceedings of the International Workshop organized by the Czech Group of the IAGOD, Prague, 10–11 September, 2002, Czech Geological Survey, Prague, pp 107–110

René M (2008) Anomalous rare earth element, yttrium and zirconium mobility associated with uranium mineralization. Terra Nova 20:52–58

Rieder M, Cavazzini G, D'yakonov Y, Frank-Kamenetskii VA, Gottardi G, Guggenheim S, Koval PV, Müller G, Neiva AMR, Radoslovich EW, Robert JL, Sassi FP, Takeda H, Weiss Z, Wones DR (1998) Nomenclature of the micas. Clays Clay Miner 46:586–595

Rubin JN, Henry ChD, Price JG (1993) The mobility of zirconium and other immobile elements during hydrothermal alteration. Chem Geol 110:29–47

Savin SM, Lee M (1988) Isotopic studies of phyllosilicatess. In: Bailey SW (ed) Hydrous phyllosilicates. Rev Miner 19:189–223

Schulmann K, Ledru P, Autran A, Melka R, Lardeaux JM, Urban M, Lobkowitz M (1991) Evolution of nappes in the eastern margin of the Bohemian Massif: a kinematic interpretation. Geol Rundsch 80:73–92

Schulmann K, Thompson AB, Jezek J (1999) Crustal thickening and exhumation in the Moldanubian zone. Terra Nostra 99:1

Schulmann K, Kröner A, Hegner E, Wendt I, Konopásek J, Lexa O, Štípská P (2005) Chronological constraints on the pre-orogenic history, burial and exhumation of deep-seated rocks along the eastern margin of the Variscan orogen, Bohemian Massif, Czech Republic. Am J Sci 305:407–448

Sheppard SMF (1986) Characterization and izotopic variations in natural waters. In: Valley JW, Taylor JHP, O'Neil JR (eds) Stable isotopes in high temperature geological processes. Mineralogical Society of America, Chelsea, pp 165–183

Skoček V, Šmejkal V, Král J, Hladíková J (1977) Isotopic composition of carbonates and sulphates from the Permo-Carboniferous of central Bohemia and the Krkonoše-piedmont Basin. Bull Czech Geol Surv 52:1–11

Stevens RE (1946) A system for calculating analyses of micas and related minerals to end members. Bull Geol Surv USA 950:101–119. Washington D. C.

Sverjensky D (1987) The role of migrating oil field brines in the formation of sediment-hosted Cu-rich deposits. Econ Geol 82:1130–1141

Suzoki T, Epstein S (1976) Hydrogen isotope fractionation between OH-bearing minerals and water. Geochim Cosmochim Acta 40:1229–1240

Tajčmanová L, Konopásek J, Schulmann K (2006) Thermal evolution of the orogenic lower crust during exhumation within ma thickened Moldanubian root of the Variscan Belt of Central Europe. J Metamorph Geol 24:119–134

Thiele O (1976) Zur Tektonik des Waldviertels in Niederoesterreich (suedliche Boehmische Masse). Nova Acta Leopold 45:67–82

Tollmann A (1982) Grossraumiger variszischer Deckenbau im Moldanubikum und neue Gedanken zum Variszikum Europas. Geotekton Forsch 64:1–91

Turpin L, Ramboz C, Sheppard-Simon MF (1981) Chemical and isotopic evolution of the fluids in the Sn-W deposit, Panasqueira, Portugal. Terra Cognita, Special Issue, p 42

Turpin L, Leroy JL, Sheppard SMF (1990) Isotopic systematics (O, H, C, Sr, Nd) of superimposed barren and U-bearing hydrothermal systems in a Hercynian granite, Massif Central, France. Chem Geol 88:85–98

Van den Kerkhof AM, Thiery R (2001) Carbonic inclusions. Lithos 55:49–68

Vilhelm S, Bajer B, Hájek A, Halík L, Hejtmánek J, Konopásek R, Chrást M, Křivánek K, Kubeček J, Mach J, Nohál M, Pesch J, Bullová J, Rozhoň V, Šenk M, Uhlík Z, Vokoun J, Žváček B (1984) General evaluation of the uranium reserves at the Rožná-Olší ore field. Czechoslovak Uranium Industry Technical Report 123-84, p 345

Vencelides Z (1991) Sulphide and barite mineralization at the Rožná deposit. MSc Thesis, Charles University, Prague, p 112 (in Czech with English abstract)

Vosteen HD, Weinoldt M (1997) Flüssigkeitseinschlußpetrographie und geochemische Untersuchungen zur Entstehung der Uranlagerstätte Rozna/Tschechische Republik. MSc Thesis, Technische Universität Clausthal, p 125

Wilde AR, Mernagh TP, Bloom MS, Hoffmann ChF (1989) Fluid inclusion evidence on the origin of some Australian unconformity-related uranium deposits. Econ Geol 84:1627–1642

Wilkinson JJ, Jenkin GRT, Fallick AE, Foster RP (1995) Oxygen and hydrogen isotopic evolution of Variscan crustal fluids, south Cornwall, U.K. Chem Geol 123:239–254

Wilson NSF, Stasiuk LD, Fowler MG (2003) Post-mineralization origin of organic matter in Athabasca unconformity uranium deposits, Saskatchewan, Canada. In: Cuney M (ed) Uranium geochemistry 2003. University H. Poincaré, Nancy, pp 383–384

Žák K, Dobeš P, Kříbek B, Pudilová M, Hájek A, Holeczy D (2001) Evolution of fluid types at the Rožná uranium deposit, Czech Republic. Stable isotope and fluid inclusion study. In: Piestrzyński J (ed) Mineral deposits at the beginning of the 21st century. Balkema, Lisse, pp 109–113

Zang W, Fyfe WS (1995) Chloritization of the hydrothermally altered bedrocks at the Igarapé Bahia gold deposit, Carajás, Brasil. Miner Depos 30:30–38

Zheng YF (1993) Calculation of oxygen isotope fractionation in hydroxyl-bearing silicates. Earth Planet Sci Lett 120:247–263

Ziegler PA (1996) Geological atlas of Western and Central Europe. Shell, Hague, p 130